2018-01-01

Evaluating Fold And Thrust Systems Within An Inverted Basin: Indio Mounntains, West Texas

Myra Guerrero
University of Texas at El Paso, guerrero.myra@gmail.com

EVALUATING FOLD AND THRUST SYSTEMS WITHIN AN INVERTED BASIN: INDIO MOUNNTAINS, WEST TEXAS

MYRA GUERRERO

Master's Program in Geological Sciences

APPROVED:

Terry Pavlis, Ph.D., Chair

Laura Serpa, Ph.D.

Jerry Johnson, Ph.D.

Charles Ambler, Ph.D.
Dean of the Graduate School

EVALUATING FOLD AND THRUST SYSTEMS WITHIN AN INVERTED BASIN: INDIO MOUNNTAINS, WEST TEXAS

by

MYRA GUERRERO, B.S.

THESIS

Presented to the Faculty of the Graduate School of

The University of Texas at El Paso

in Partial Fulfillment

of the Requirements

for the Degree of

MASTER OF SCIENCE

Department of Geological Sciences

THE UNIVERSITY OF TEXAS AT EL PASO

August 2018

Acknowledgements

This journey would have not possible without the support and encouragement from my professors and peers. I would like thank Dr. Terry Pavlis, who always believed in my ability as a geologist. Despite life's many obstacles, Terry continuously encouraged me to keep going. I am very grateful to have had him as my advisor. I would also like to thank Dr. Laura Serpa, who was always patient and always ensured I had everything that I need to complete this project. I also thank Dr. Jerry Johnson for providing comfortable place to stay in the middle of the desert, delicious meals, and interesting insights to the biological world of the Indio Mountains. I thank Dr. Jose Hurtado for taking the time to come out and teach me the valuable skill of flying drones.

Special thanks, to my husband, Christopher Salas-Zuniga, for pushing to finish and even carrying the gravimeter for miles just for me. Thank you, Jose Pablo Cervantes, Samantha Ramirez, Victor Avila, and Raquel Guzman for taking the time to go out into the field and provide input and thought-provoking ideas as to what you thought of this complicated area, despite working on your own projects. Thank you, to Felix Ziwu for greatly helping in the geophysical aspect of this project, and for always pushing me to do better.

Thank you, all. To God be all the glory, honor, and praise.

Abstract

Fold and thrust belts often are complicated by out of sequence thrust faulting and inverted basins display these structures particularly often due to reactivation of original normal faults as well as complex topographic evolution. The Indio Mountains lie along the northern margin of the Chihuahua trough which formed as a mid-Cretaceous extensional basin and was subsequently shortened during the Laramide orogeny, making the Indio Mountains an exceptional site for studies of structures produced by large scale basin inversion. This study focuses on the subsurface structures in a complexly imbricated thrust window developed along the paleo rift basin margin.

This study examines the area through a multi-method research approach that includes: a) new or improved definition of stratigraphic units/subunits within the Cretaceous Yucca formation; b) the production of a geologic map from surface rock exposures; c) the collection of geophysical data and processing; d) the construction of a 3D model of the area. Through this data the study characterized a fold-thrust system developed in an inverted system and evaluated the role of out of sequence thrust faults involved, correlated with geophysical modeling, and assessed models for thrust systems in these tectonic settings. There is worldwide demand for rational and thorough subsurface geologic models, particularly in inverted basins which are commonly major hydrocarbon producers. Recently 3D mapping programs have been employed to improve subsurface resolution but despite the demand the process is in its infancy (Russel et. al., 2013). The resulting 3D model greatly served as an improved digital elevation model (DEM). Gravity analysis resulted in small changes, yet nonetheless correlated well with surface geology and fault associations. Overall, the collective of data resulted in the geologic interpretation of an

extremely shallow upper plate duplex, and ambiguous thrust sheet identification due to severe deformation in the area.

Table of Contents

List of Figures

List of Plates

1. Introduction

The goal of this study was to better understand the kinematics of inverted basins and their association with fold and thrust systems. Inverted basins are collectively a result of an intricate interaction of the extension and shortening of shallow sedimentary layers (Lowell, 1995). The geological structure of the Indio Mountains has been subject to few studies and remains to poorly understood, yet, the Indio Mountains are an optimum setting for study of basin inversion due multiple exposure levels produced by Neogene extension and location along the boundary of a Mesozoic rift basin that inverted during Laramide contraction.

Although early studies recognized the typical stacking sequence of fold thrust belts with thrust younging toward the foreland, it has become increasingly apparent that many fold and thrust belts display out-of-sequence thrust faulting (Morley, 1988). Out of sequence thrust faults illustrate rejuvenation of deformation in the hinterland and are caused by reactivating preexisting faults and or by creating new ones (Morley, 1988). These faults are found in the orogenic wedge of the thrust system and theoretical studies indicate they form to maintain the critical taper when the mechanical conditions change over time (Chapple,1978; Dahlen, 1984). Out of sequence faults are also indispensable features of thin-skinned folding or deformation of the weak basal layer (Morley, 1988; Chapple, 1978). Unlike thrust faults which place older on younger rocks as they are transported up section (Fox, 1969), out-of-sequence thrust faults commonly put younger on older rocks both up and down section (Morley,1988; Pavlis, 2013). Another commonality linked with out-of-sequence thrust faults is their association with the deformation of marine sedimentary rocks (Morley,1988). Although thin vs thick skinned deformation instances are geologically well known (for example in the Malargüe fold-and-thrust belt; Giambiagi et. al.,

2008), the geometries resulting in out-of-sequence thrusting are far less researched due their considerably difficult kinematics and uncertainty involving their reconstruction (Pavlis, 2013).

Inverted structures are common traps for hydrocarbons and are often controlled by the strength and kinematics of inversion tectonics, but still not well understood (Yang, 2011). Today, oil exploration has vastly improved by utilizing advanced technologies, such as 3D modeling. Due to high costs, however, it is imperative that information is abundant and interpretation is correct (Caumon, 2009) and exposed examples are important in this context. The Indio Mountains serves as an analog to an offshore inverted basin (Page, 2011) for which the proper interpretation and methods may aid future studies.

In addition to the importance of structural traps linked with inverted basins, this study also illustrates the utilization of 3D modeling for structural analysis and the pros and cons associated with that process. Also, it is universally known that structural tendencies and geometries from inversion are more complicated than simple imbricated thrusts and range from a variety of small and large thrust systems (McClay, 1992). Thus, for this study the inclusion of geophysical gravity data serves to support in the structural interpretation of the poorly resolved Laramide structures of the Chihuahua trough.

This paper sets a new foundation for geologic mapping of the central Indio Mountains (Figure 1) through new detailed mapping and 3D analysis of a complex klippe-fenster system that displays characteristics indicative of out-of-sequence thrusting. We build a new interpretation of the structural geometries and kinematics of the fold and thrust systems associated with this inverted basin system; supplemented by a gravity survey map and updated geologic map.

2. Geologic Setting

The Indio Mountains have a geologic history as part of the Chihuahua trough (Figure 2), which is an inverted extensional basin exposed in the northeastern part of Chihuahua Mexico, southwestern Texas, and southern New Mexico (Figure 2) (Haenggi, 2001). The Chihuahua trough has a multifaceted history with a general lack of understanding of its geologic systems (Haenggi,2001; Page, 2011). Tectonic activity in the region began in the late Paleozoic during a collisional -subduction event as Larentia subducted beneath the northward motion of the South American side of Gondwana (Poole et. al., 2005). This collision produced the Ouachita-Marathon-Sonora orogeny, a 3000 kilometer-long belt of deformed Paleozoic rocks ranging from Early Paleozoic to Permian in Texas, Chihuahua, and Sonora (Poole et. al., 2005). Synorogenic strata in this late Paleozoic orogen young westward in foredeeps that are interpreted as oblique suturing between the craton and Gondwana (Poole et. al., 2005). The orogenesis ended diachronously in the Ouachita Mountains and the Marathon region, between the late Pennsylvanian and Early Permian (Poole et. al., 2005).

Following these events, North America moved westward relative to Gondwana. During the Jurassic, the north Atlantic breakup presumably transferred as sinistral-oblique slip across what is now northern Mexico (Anderson, 1983; 2005). The Chihuahua trough likely was initiated during this Jurassic period (e.g. Haenggi, 2002). The key rifting in the Chihuahua trough occurred during middle Cretaceous time when the main syn-rift sedimentary sequence was deposited (Haenggi , 2002). The origin of the Cretaceous rifting is debated. Dickinson and Lawton (2001) considered this rifting a back-arc spreading event whereas Haenggi (2002) interpreted a right lateral pull-apart basin origin for the Chihuahua trough (Haenggi, 2002). Nonetheless, during the Mesozoic rifting, the Gulf of Mexico subsided, allowing the Tethy's

Ocean marine waters to migrate northward and filling the growing Chihuahua trough (Carciumaru, 2006; Dickinson 1981).

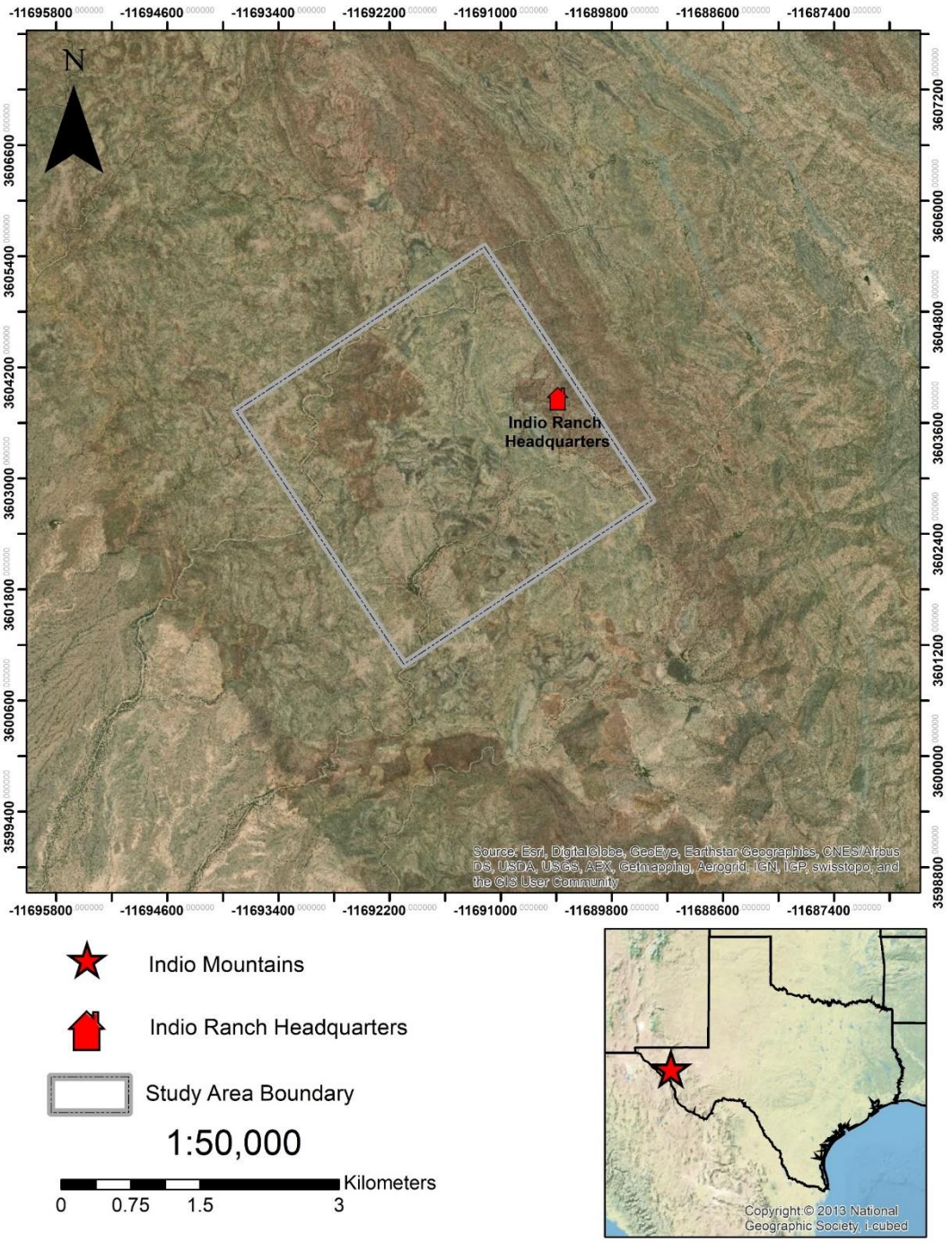

Figure 1: A general map depicting the location of the Indio Mountains in Texas, the Indio Ranch Headquarters, and the study area.

Late into the Jurassic the Chihuahua trough region became the site of evaporite deposition that played a major role in subsequent deformation (Figure 2) (Haenggi, 2002). During the mid-Cretaceous, the rift rejuvenated with deposition of coarse, nonmarine conglomerates along the basin margins, but ultimately as sea level rose during the global Cretaceous sea level rise, the area experienced marine carbonate deposition and active rifting ceased (Haenggi, 2002; Li, 2015).

The Chihuahua trough was later inverted during the Laramide Orogeny (84-43ma) as basin boundary faults were reactivated as thrust faults with northeast-southwest compression (Haenggi, 2002). The compression of the Chihuahua trough has led to several hypotheses on the dynamic thrust and fold systems coupled with the Laramide Orogeny. The first involves a single major occurrence where the deformation of the eastern region took place during the late Paleocene (Wilson, 1971; Carciumaru, 2006). On the other hand, Maxwell et al. (1967) proposed the occurrence of several episodes of folding, with the primary event of linear regional uplift and the later event(s) of folding and thrust faulting.

During Laramide orogenesis sedimentary rock packages piled up against the Diablo Platform as a series of thrust sheets, producing intense structures that include low angle thrusts and overturned folding (Carciumaru, 2006). Although Laramide Compression for the southwestern US is commonly linked to subduction of two oceanic plateaus in Late Cretaceous and Paleogene time, this hypothesis is difficult to reconcile with Laramide contraction is most of Mexico and the thin skinned thrust systems of the border region. Carciumaru, (2006) suggested that compression was due to the subduction of the Farallon plate beneath the North American plate, producing northwest trending thrust faults and folds. Alternatively, Fitz-Díaz et al. (2017) have suggested this Mexican/border region Laramide contraction is related to collision of the

Guerrero terrane with western Mexico. Other hypothesis, are dependent on the widely debated motion of the Farallon Plate, in which compression direction drives the regional tectonics. The first being northeastern compression and transport resulting in folding and northwest trending fault systems (Underwood, 1962; Page, 2011). The second illustrates the pragmatic northeast-southwest trending folds to be the product of transpression tectonics (Dickerson, 1985; Page 2011).

Around 31 Ma regional stresses switched from compressional to extensional (Henry et. al., 1991; Haenggi, 2002). Following the Laramide Orogeny extensional block faulting, presumably part of the Basin and Range development and younger Rio Grande rift system, overprinting the contractional structures (Haenggi, 2002).

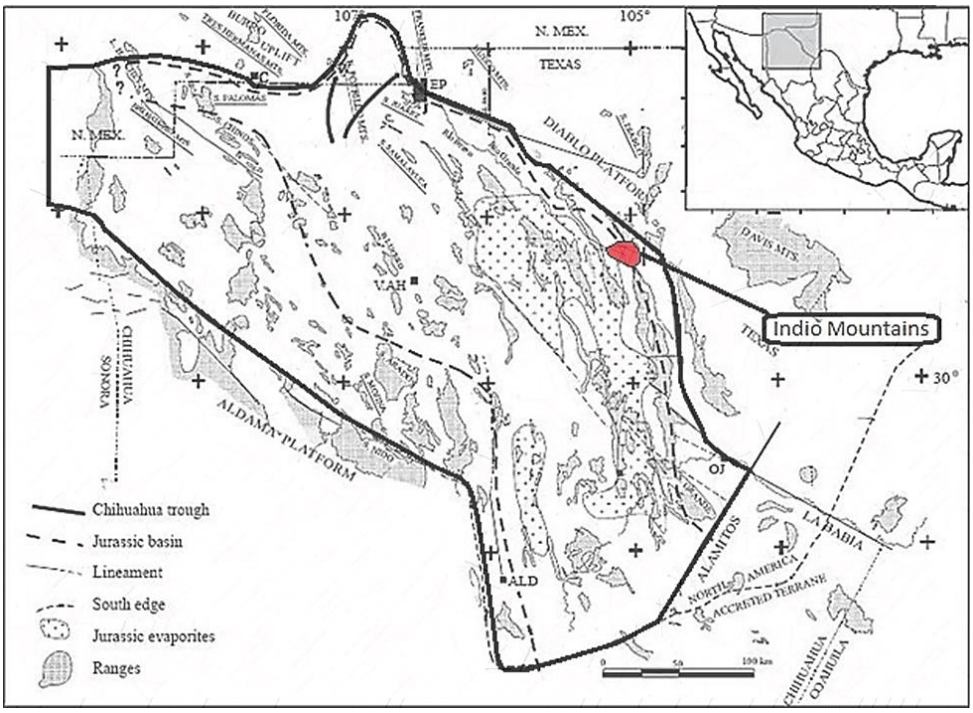

Figure 2: Outline of the Chihuahua trough, bound by the southwest Aldama, Alamitos lineament, and northeast Diablo platforms (modified from Carciumaru, 2006). Red boundary signifies Indio Mountains area.

3. Geology of Indio Mountains

3.1 Stratigraphy

The oldest unit exposed in the central Indio Mountains is the Yucca formation which can be divided into two subunits, the lower and the upper Yucca (Page, 2011; Underwood, 1962), but further division is also possible (Fox, 2016, Ramirez, 2018). The lower Yucca unit is a thick conglomerate with a reddish or light grey matrix, and contains white, black and pink pebble sized clasts (Page, 2011). The conglomerate is interbedded with thin layers of a cross-bedded greenish quartzose sandstone, and minor red-purple shale layers (Smith, 1940). Campbell (1980) interpreted this unit as a lacustrine, bay, or lagoon depositional setting and the upward fining through the entire Yucca formation as a coastal plain fluvial environment. More recently, Page (2011) and Li (2015) suggested the opposite with the lower section interpreted as fluvial deposits and the upper section as coastal marine (Page, 2011) or lacustrine/fluvial interbeds (Li, 2015).

Page (2011) used an informal division between the lower and upper sections at an approximate stratigraphic level where the dark maroon color of the lower unit transitions to an alternating white and maroon colored rocks that also marks a general fining to sandstone-dominant rocks. He interpreted this line as the transition in depositional environments from fluvial to coastal marine, but more recent work (Li, 2015) suggests a transition to a mixed fluvial-lacustrine system within a coastal environment.

The upper Yucca formation is lithologically very diverse. The sequence is dominantly clastic with a predominance of medium to fine sandstone, but the sandstones are interbedded with limestone, maroon siltstone and shales (Page, 2011) that show dramatic lateral facies variations (Li, 2015). This unit contains a number of distinct sedimentary facies including

diamictite horizons that presumably represent debris flows, unusual ripple-laminated fine sandstones, and red shales with large limestone nodules (Li, 2015).

The Yucca formation is conformably overlain by the Bluff Mesa formation which is composed primarily of limestones interbedded with white to brown quartz arenite sandstone (Page, 2011). Page (2011) divided the Bluff Mesa formation into three members, a lower, middle and upper unit (Figure 3). The lower member is a massive gray fossiliferous limestone accompanied with oolitic beds and a fossil called Orbitolina (Page, 2011). The middle member consists of interbedded limestones and quartz-arenite sandstones, which closely resemble that of the overlying Cox sandstone and underlying sands of the upper Yucca formation (Page, 2011). The upper member is similar to the lower member with an abundance of Orbitolina fossils but characterized by an abundance of shale as well as distinctive bluish grey massive limestone layers (Page, 2011).

3.2Structures

Along the US-Mexico border in west Texas the entire Chihuahua trough takes on a bowed-shape, arched easterly toward the Diablo platform, against which the thrust systems impinged in the Laramide. The Indio Mountains mimic the same shape at a smaller scale and folds and thrust systems conform to this regional pattern. Associated with this shape variation structural trends vary from the north to the south. The Indio Mountains therefore seem to be the result of a thrust sequence produced by west to east contraction (Page, 2011). Commonly with arcuate salients in thrust systems contraction begins perpendicular to the mountain belt but becomes more radial as deformation progresses (Tibaldi, 2018). Thus, in the Indio Mountains, northern structures trend northwest-southeast, become progressively northing at the salient, and trend northeast-southwest to the south (Page, 2011; Carciamaru, 2006).

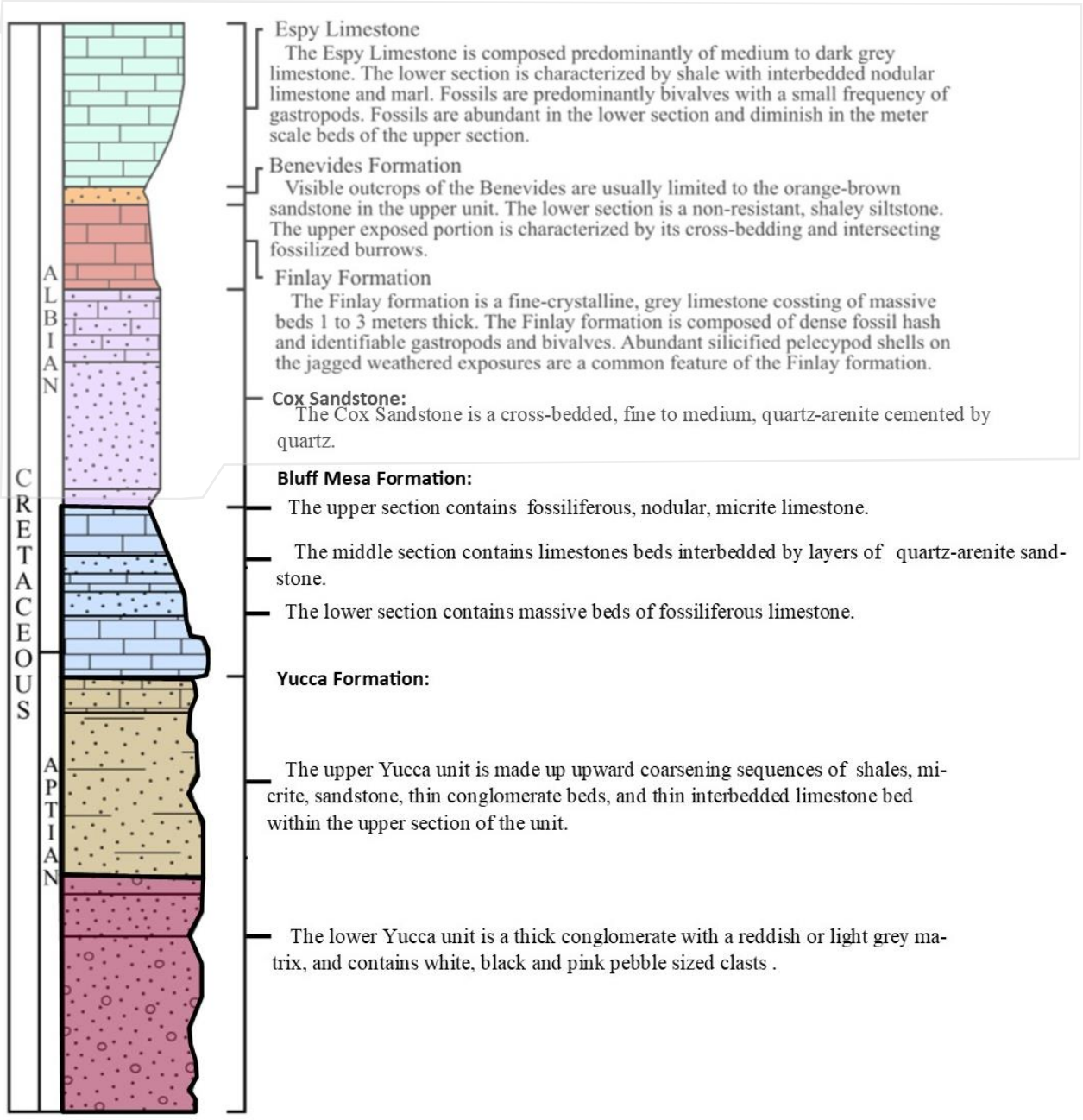

Figure 3: General stratigraphic column of rocks found in the Indio Mountains (modified from C Underwood, 1962; Rohrbaugh, 2001; and Page, 2011).

Normal faulting overprinted the contractional structures and these faults exhume different structural levels across the region. In the mapped area the most conspicuous of these normal faults is the Indio Fault which divides the area into two distinct structural domains (Figures 4 and 5). To the west of the Indio Fault, however, two important normal faults also cut the section,

forming a horst block (Figure 6) bounded on the west by Borrego Fault and on the East by the Red Mountain Fault (Ramirez, 2018). These normal faults continue northward into the mapped area of this study (Plate - 1).

East of the ranch house is the Indio fault. The Indio Fault footwall to the east was mapped in the early 1960's by Underwood (1962) (Figure 4) and more recently by Page (2011) (Figure 5). The footwall contractional structures are large and were misinterpreted in early studies by Underwood (1962). Two major thrusts, the Squaw Peak and Bennett, were mapped by Underwood (1962) with the Squaw Peak thrust structurally overlying the Bennett thrust. The Bennett thrust emplaces the Yucca formation over the Bluff Mesa to Espy formations with the thrust cutting upsection toward the east in the footwall. Underwood (1962) interpreted the Bennett fault to be a back thrust, but this interpretation is inconsistent with the footwall cutoff geometry. Thus, Page interpreted the Bennett as the upper thrust of a duplex with the Squaw Peak thrust as the roof to the duplex. Page (2011) also inferred that the entire thrust system was underlain by a decollement at depth that potentially surfaces as a frontal thrust in the Van Horn Mountains.

Page (2011) also mapped part of the Indio fault hanging wall (Figure 5), but recognized this area was complexly deformed by both overturned, east-vergent folds and half-klippen of a thrust system truncated to the east by the Indio Fault near the Indio Ranch House. Page (2011) correlated the thrust beneath this half klippe as part of the Squaw Peak thrust system, a hypothesis that is evaluated further here. Pages's (2011) work made it clear that significant structural complexities exist in the hanging wall of the Indio fault, in the vicinity of the Ranch House (Figure 5), which partially inspired this study.

3.3 Folds

Numerous folds are recognized in the Indio Mountains and include a variety of fault-related fold systems (Page, 2011). Large broad folds are recognized in the hanging wall of large thrust systems and generally represents fault-bend folds (Page, 2011). Both detachment and fault-propagation folds as well as drag folds combine to produce local overturned folds, such as the overturned syncline overlain by the half klippe near the ranch house (Page, 2011). Drag folds also are found adjacent to steeply dipping normal faults but are not significant to this study.

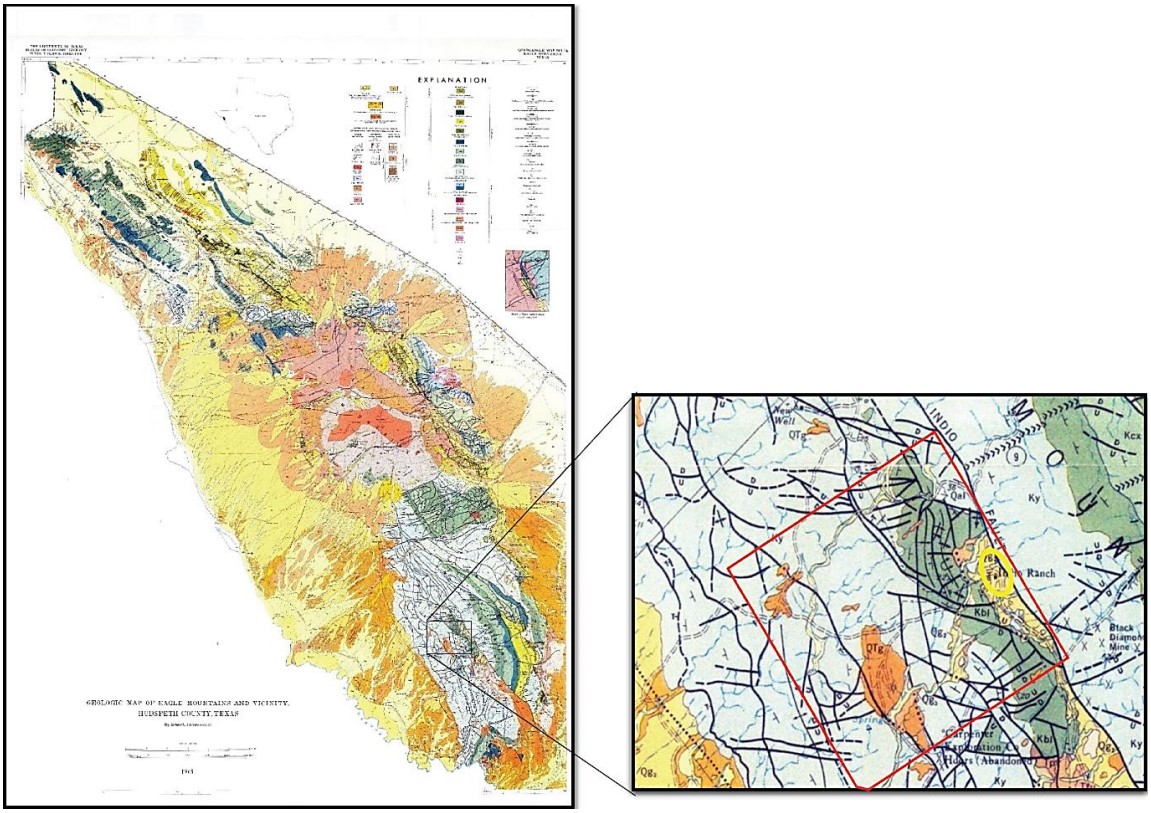

Figure 4: Geologic map of the Eagle Mountains and the adjacent areas (Underwood, 1962), and a close-up view of the area mapped. The area of study lines in the Indio Mountains and outlined in red.

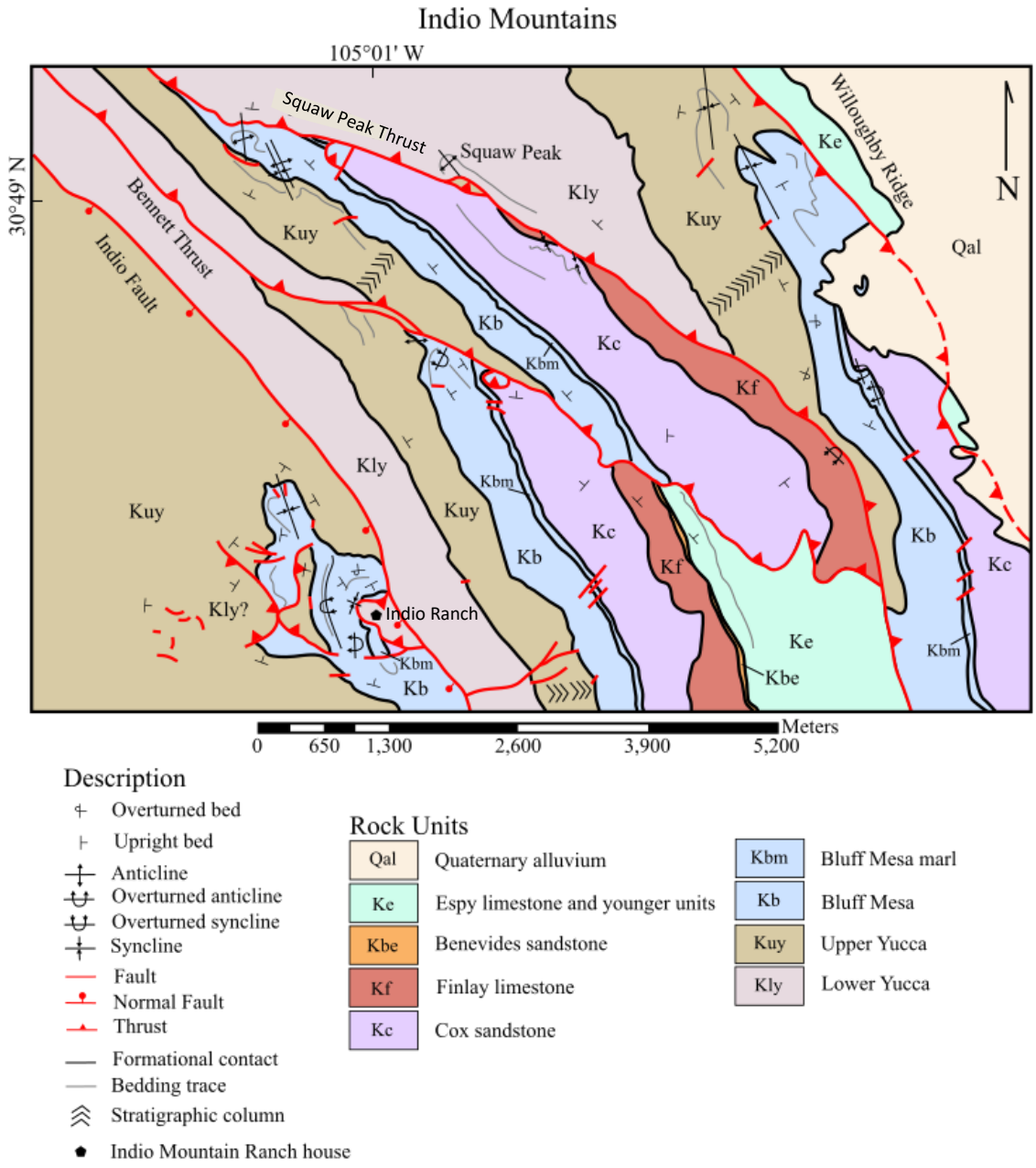

Figure 5: Geologic map of eastern footwall of the Indio normal fault, modified from Page (2011). dashed line indicates study area.

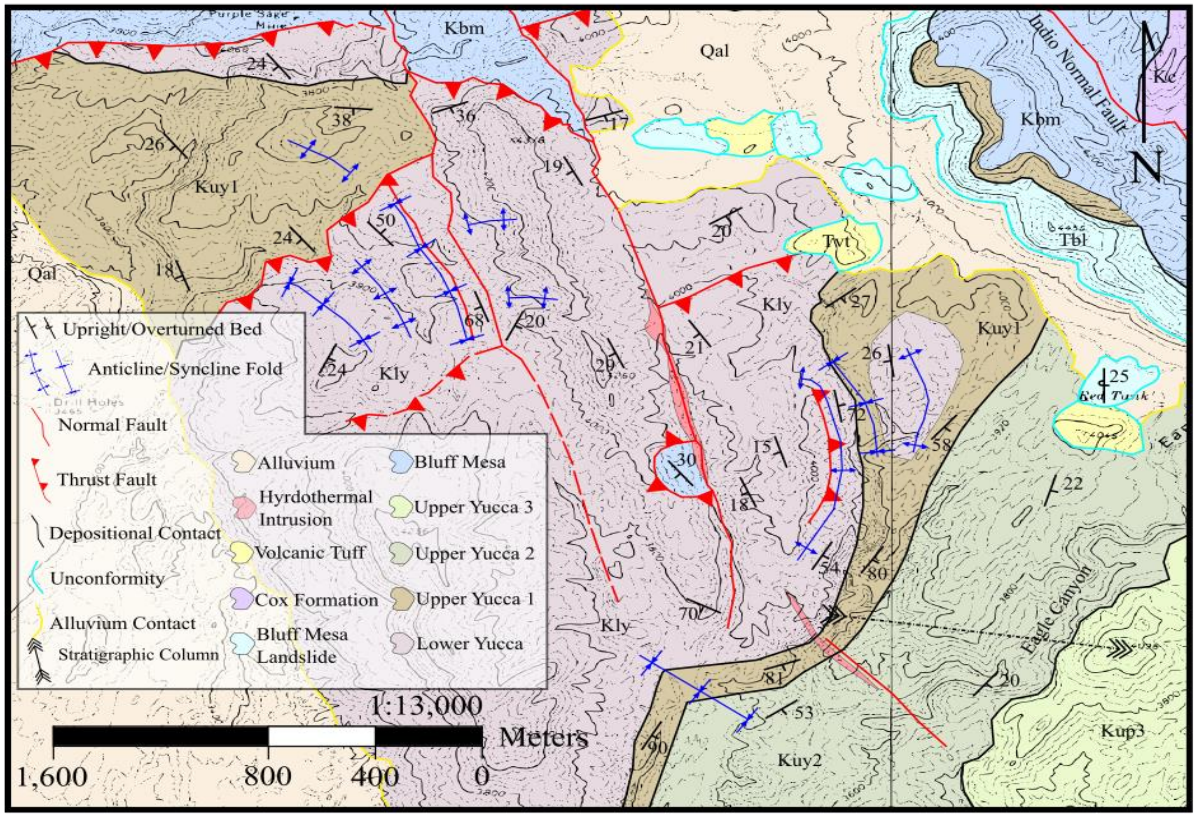

Figure 6: Geologic map of south region of the hanging wall of the Indio normal fault, modified from Ramirez (2018).

4. Methods

This study was achieved through comprehensive geologic analysis that included stratigraphic studies, advanced geologic mapping, 3D visualizations/models, and geophysical methods. With the only published map dating back to the early 1960's (Underwood, 1963) (Figure 4), prior to the introduction of many modern concepts of fold-thrust system development, the area west of the Indio Mountains was chosen in an effort to update the geologic map of the area. In addition, previous reconnaissance by T. Pavlis and R. Langford had established the area was structurally complex and thus, the area was chosen to apply new advanced mapping techniques to better understand the structure. Research was done in three key phases: 1) Gravity Survey, 2) advance geologic mapping, and 3) 3D modeling.

4.1 Gravity Survey

Geophysical methods used to constrain subsurface structural geometry employed a gravity survey of the area (Figure 7). A 3x3 kilometer grid was used with points equally spaced 250 meters apart throughout the area, resulting in 90 points (Figure 7). The gravity data were obtained using *a LaCoste and Romberg* gravimeter and *TopCon GB1000* GPS equipment for precise positioning to the centimeter level. Prior to the gravity survey a GPS and gravity base were established at the Indio Mountain property fence entrance Indio Ranch Headquarters. To obtain a gravity value for the base station multiple loops where conducted, first from the Van Horn post office to the Indio Mountain property fence entrance, and from the fence to the ranch. Following field data collection, the gravity data were processed using *Microsoft Excel* in order to obtain the Simple Bouguer Anomaly. The final data was then imported into *Oasis Montaj* where the data a terrain correction was applied resulting in the final Complete Bouguer Anomaly. In order to constrain the data further a Bouguer residual map was generated by subtracting a third

order polynomial to remove regional gravity affects. Processed data were then converted into a raster file using *Oasis Montaj* for modeling and ultimately transferred to *ArcMap version 10.3*.

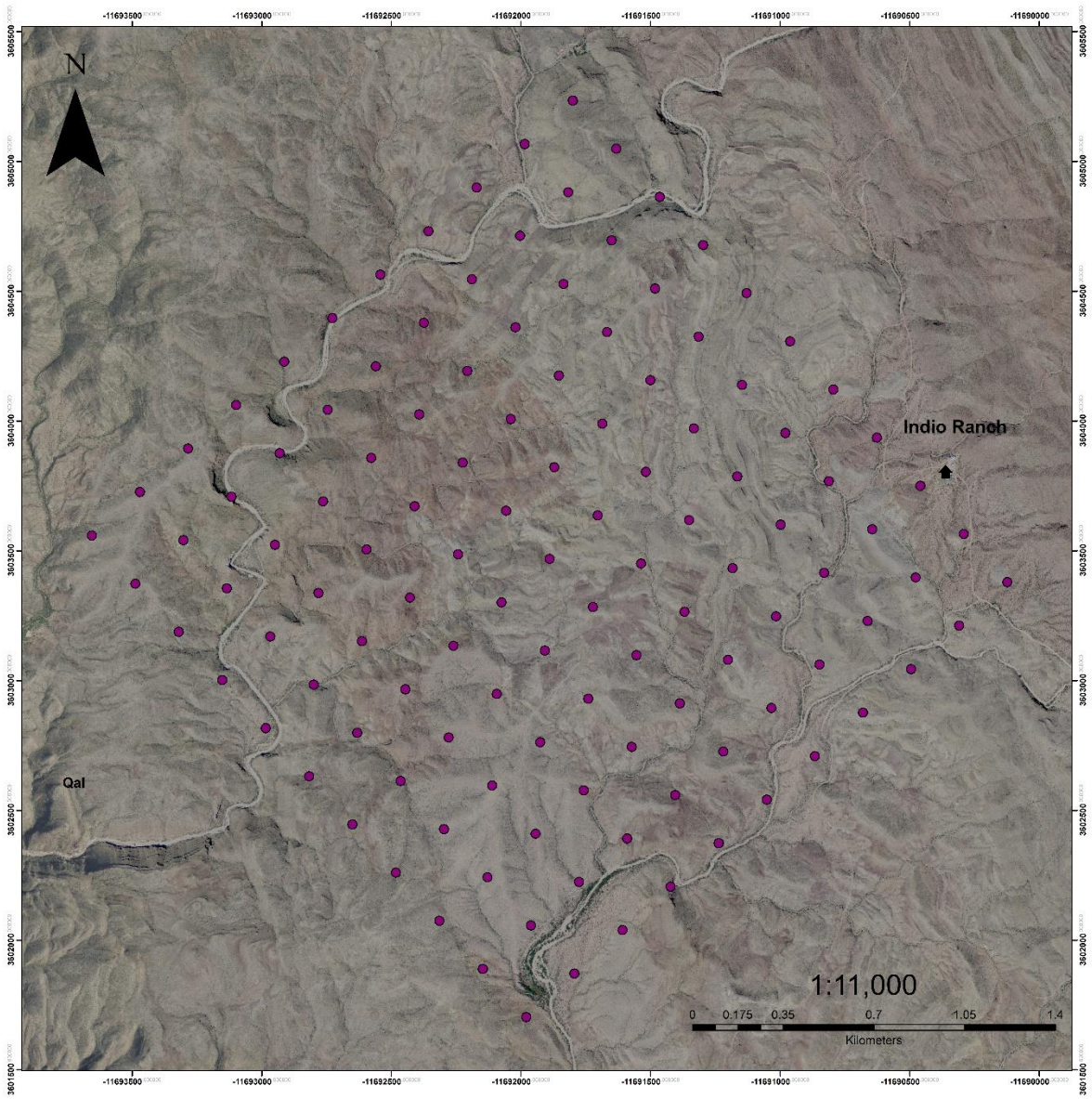

Figure 7: Gravity survey point grid plotted over the study area on an orthophoto base. A total of 90 points (purple) equally spaced ant 250 meters apart.

4.2 3D Modeling

Because of the areas structural intricacies this study attempted to construct a 3D terrain model at centimeter resolutions using an aerial, drone-based surveying technique. In order to begin creating the 3D model at such a large scale a set of grid points were generated using the Fishnet tool in ESRI's *ArcMap*. The tool overlaid a geographical point grid over the area with 500 meter spacing (Figure 8). These points served as essential ground control points or marker points that were used to identify locations within photos, and ultimately provide georeferenced indicator to which the photos align within the processing stages (Brush, 2015; Stojakovic, 2008).

With previous experience in the *Agisoft PhotoScan* photogrammentry software, the use of natural objects as marker points was not efficient, in a way that both the program and the user have difficulty identifying the ground control points in the photos. Thus, a grid map was generated in which each row of points was given one symbol and the columns where assigned a particular color (Figure 8). This method was chosen to aid not only the processing but the user when picking points and processing data. In order to transfer these colorful symbols to be utilized in the field and serve as ground control points, colored cornstarch and plates were used to essentially draw these symbols on the ground at about 1 meter wide.

Autonomous drone flights were conducted within a 500x500 meter grid square using *3DR* drone with a fixed mount pointing perpendicularly to the ground a surface. A *Hero 3 GoPro* camera set to take 1080-pixel video was used to acquire the imagery. Flights were planned using the *Mission Planner* software, where altitude was set to 80 meters relative to the surface and was set to collect images with 50 percent overlap.

Following the infield flights the videos were extracted from the camera and converted into photos using a free online video to jpeg application. The photos were generated in three

different time intervals every: 1 seconds, 10 seconds, and 30 seconds. To preserve at least 50% of the overlap the photos/10sec.s were used in *Agisoft PhotoScan*. The *Agisoft Photoscan* workflow consists of several steps. The first few steps address photo setup, alignment and adjustment, while the next several steps cover error reduction and bundle adjustment. The final steps allow the user to build dense point clouds, meshes, texture DEMs and orthomosiacs.

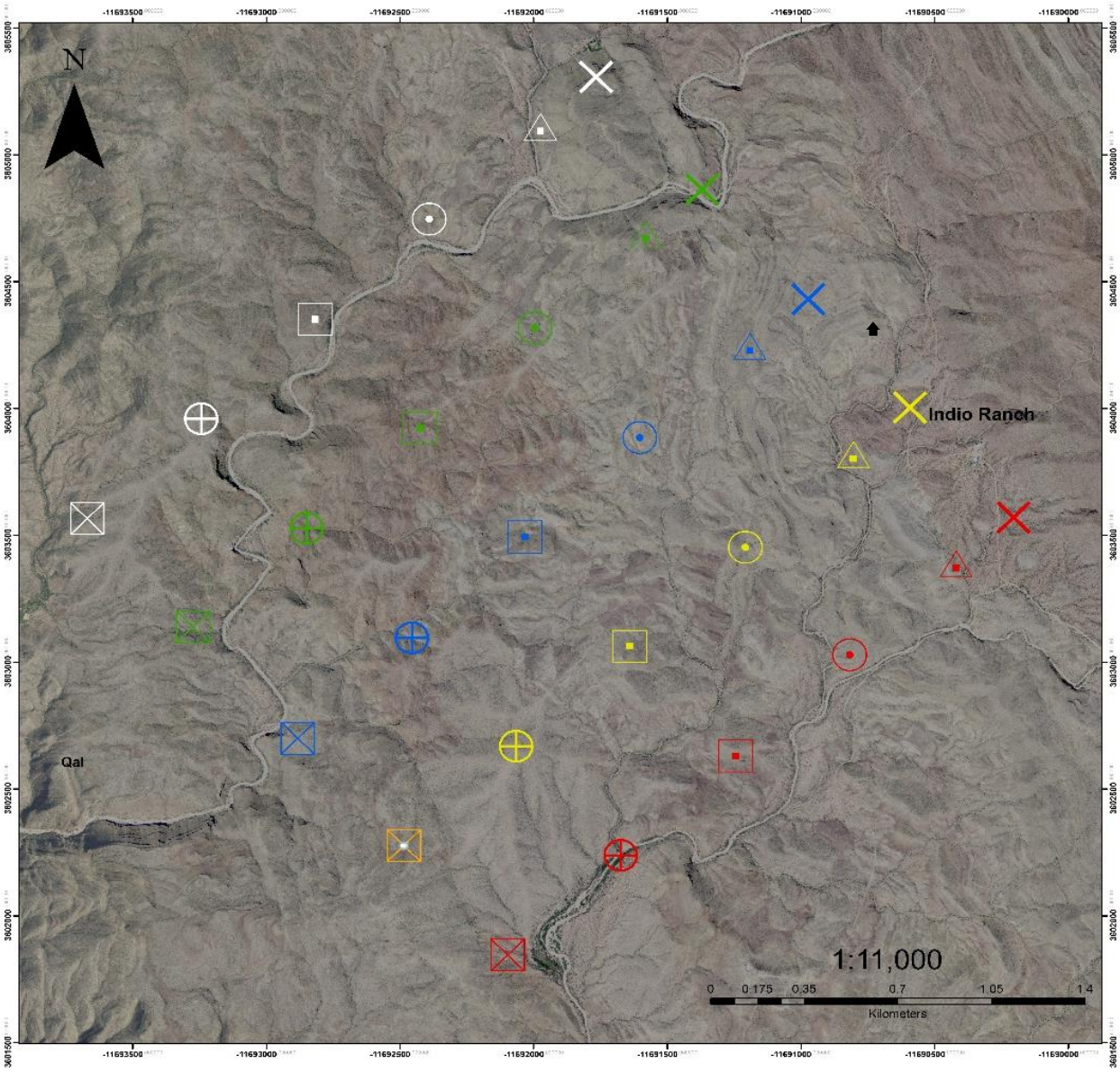

Figure 8: Point marker grid with coordinated and symbols and colors for accurate model georeferencing. Points were located using high resolution GPS.

Photo setup, alignment and adjustment is accomplished in the first five steps. Adding photos, arguably the first step, is accomplished by accessing the Main Menu > Workflow. This allows for the selection of all photos necessary for the project. The next step would be to set the coordinates and projection through the Reference Panel > Settings. The following step would be to ensure that all photos with similar focal distance and parameters are grouped together. This camera calibration can be accomplished through the Main Menu > Tools. Once grouped, the photos need to be aligned; the settings for this are high, generic or referenced, 60,000, 0. For the alignment, access the Main Menu > Workflow. The final step for photo setup, alignment and adjustment would be the initial bundle adjustment complete via Reference Panel > Optimize. Error reduction and bundle adjustment constitute the next four steps and begins with Reconstruction Uncertainty (Geometry). Set Level 10, if more than 50% of points are selected, the level must be increased to a higher value. Then the point would be optimized through their deletion.

Repeat this step at least two times while lowering the Level as close to 10 as possible without deleting more points. This can be accessed via the Main Menu > Edit and through Gradual selection. Projections goal should not be less than 100 with the Error (pix) goal of .3 SEUW 1.0. Following Reconstruction Uncertainty would be Projection Accuracy (Pixel Matching Errors). To begin, set Level 2-3. Again, if more than 50% of points are selected the level must be increased to a higher level. Delete the points, optimize. Repeat at least two more times to get as close Level 2 as possible without deleting more points. The next step is to Tighten Tie Point Accuracy Value. Change the settings of the tie point accuracy(pix) from 1 to .1 then optimize. The Projections goal should continue to be not less than 100 with Error (pix) goal of .3 and SEUW of 1.0.

Control Points (Markers) are imported by manually selecting or through auto detection on individual images. Scales bars would be added by selecting the Coordinate System (Local, Geographic, Projected) and Projection. This was done from Main Menu > Photo Edit Markers. Next was a repetition of the Reprojection Error (Pixel Residual Errors), finally followed by the building of a dense point cloud. The completion of the dense point cloud is then exported to a.LAS format, where it is then imported into the *Cloud Compare* software.

By grid square the photos were aligned via ground control points, and a high-resolution point cloud was created (Pavlis et. al., 2015) and exported into *Cloud Compare* where all points clouds were merged together to create a high resolution digital elevation model (DEM).

4.3 Field Methods

To thoroughly analyze the structures in the area, a stratigraphic column was developed for the Upper Yucca unit in collaboration with Ramirez (2018). The unit was divided into 3 members, in order to noticeably identify structural geometries within a larger unit. To preserve the dimensions of the unit thickness the stratigraphic column was purposefully done within the hanging wall of the Indio fault. Because, the Upper Yucca unit was not fully exposed and highly deformed, the stratigraphic section was recorded ~5 kilometer to the south of the study area where the unit was adequately exposed and not complicated by faults or folds.

Geologic mapping was done using modern digital mapping techniques and programs using a variant on the data structure of Pavlis et al. (2010). In order to develop the geologic surface map all data collected in the field were collected and entered into *QGIS*, running on a DELL tablet. High resolution orthophotos with a .05 meter resolution approximated initial contacts and fault lines, locations, and general surface mapping. Field work verified initial data, in which bed orientation as well as fold and fault data were collected using a classic Brunton compass. These

data were then refined in *ArcMap* version 10.3, and imported into *Move 2017, 2018,* where imagery was draped over the DEM.

When generating cross-sections, the mapped strike and dips, faults, polygons, and contact lines were imported over from *ArcMap* to the *Move* as shapefiles. This allowed to the *Move* program to maintain all aspects including geographical location of the data. Strategically. particular cross-sections lines where chosen throughout the map, and then relative data such strike and dips, fault and contact lines that crossed the section were projected onto the newly generate profile. Following this, the unit thickness was manually imputed, allowing the *Move* program to maintain the units thickness when necessary. With all the necessary data projected on to the profile, cross-sections were created which allowed clear subsurface structural visualization.

5. Results

5.1 Stratigraphy

From initial reconnaissance of the study area it was clear that the upper Yucca section was the dominant rock unit, but it was complexly deformed. Thus, to aid mapping and to better understand the structures of the area a stratigraphic section was measured to develop subdivisions of the upper Yucca (Figure 9). This section was measured in collaboration with Ramirez (2018), who reported these data, but it partially reiterated here because of its importance to this study (Figure 9).

The upper Yucca section measured approximately 580 meters in total thickness. This section was divided into three members. The basal contact of unit 1, shares another informal contact that divides the lower and upper Yucca units from massive conglomerate layers to a more facies varied and alternating sandstones and mudstone.

Unit 1 was measured to be approximately 78 meters thick; and begins with the first reddish-brown mudstone overlying the lower Yucca conglomerate. The unit is made up of upward coarsening sequences of brown laminated cross stratified burrowed fine to medium course sandstone with overlying interbedded 1 centimeter thick coarse-grained rip up clast beds. This unit is not mapped within the study are, but the understanding of the stratigraphy proved important in the determination of the unit density when creating the gravity profile.

Unit 2 is the largest of the 3 members and is measured to be approximately 364 meters thick. This unit is similar to the antecedent layer with the exception of the more abundant presences of shale beds within the unit. The base of unit 2 is mostly composed of massive orange-white medium coarse-grained sandstone with large 3-meter-thick trough cross-beds and small interbedded ½ meter laminated shale beds, and burrows found atop the upward coarsening

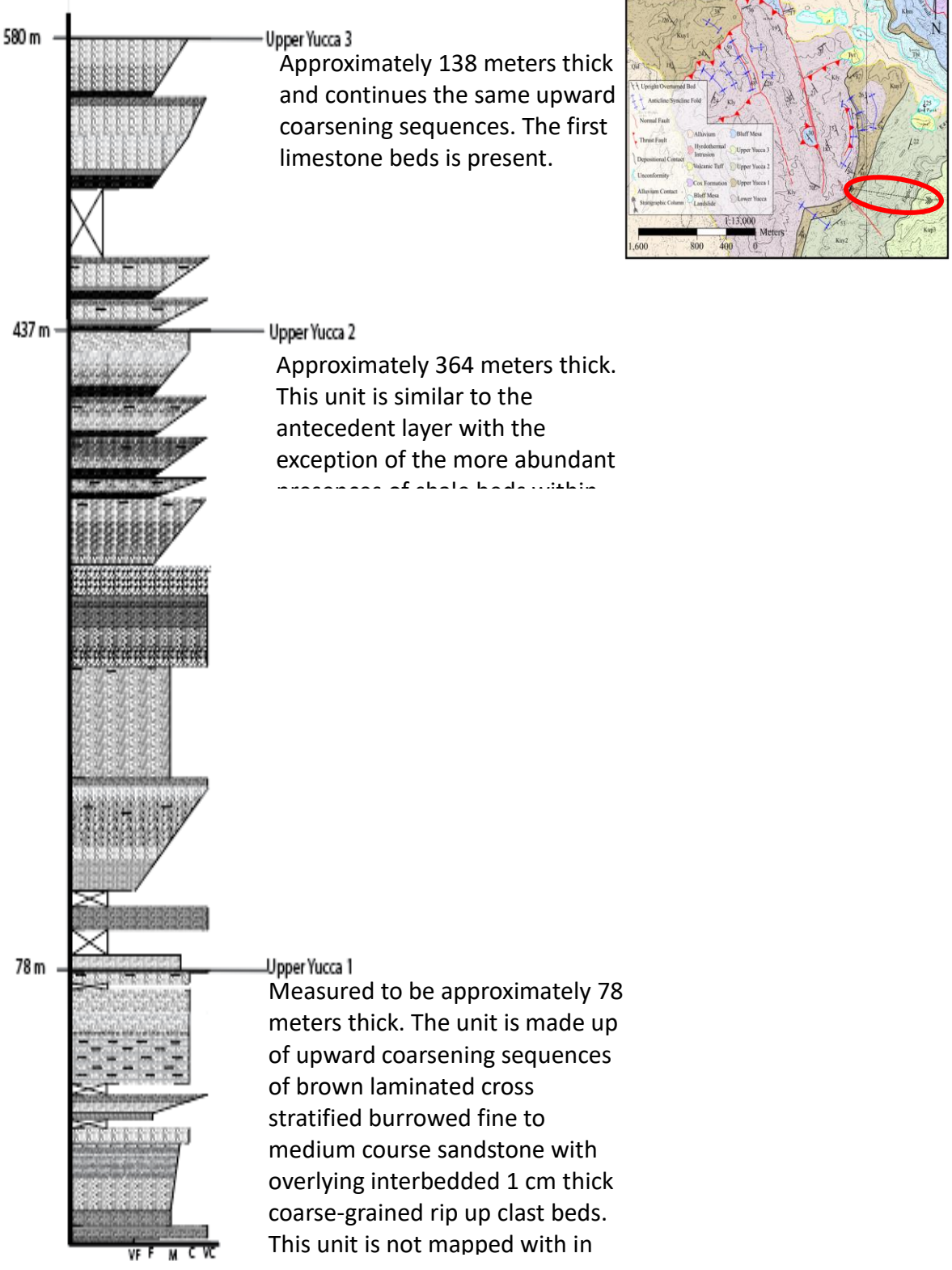

Figure 9: Stratigraphic column of the upper Yucca section.

sequences. The upper 122 meters of unit 2 begins repeated sequences of upward coarsening and the presence of lower blue-ish grey limestone nodules interbedded marron shales. This is overlaid by dark drown burrowed micrite beds, with sharp transitions to a coarse orange-white sandstone and then to 2-3 meter thick grey conglomerate beds with a coarse sandy matrix and various 5-10 centimeter thick chert pebbles. This sequence is repeat throughout the remainder of the units, yet the conglomerate beds noticeably become smaller and the limestone nodules become more evident up section.

Unit 3 is approximately 138 meters thick and continues the same upward coarsening sequences that make up the upper layers of unit 2. In unit 3, the first limestone bed is present, therefore making this unit distinguishably different from the other two units within the section. Also, there is significant reduction in the sized of the conglomerate as limestone and sandstone beds become more apparent.

5.2 3D Model

A 3D Model of the study area was constructed with the use of the *Cloud Compare* program (Figure 10), the program was used to align the various point cloud grid squares. Following the combination of the various point clouds; it was determined that the final model did not have a resolution adequate to further enhance the mapping process nor structural interpretation but depicted similar resolutions to open source models such as *Google Earth* and *ArcGlobe*. Nevertheless, a 3D model was generated (Figure 11) and the point cloud was still utilized and converted into a DEM and imported into *Move* where it aided in the creating and interpreting geological cross-sections (Figure 12).

Although, a high-resolution model was the goal, ultimately the use of a 1080 video resulted in final low resolution of the model. Had a 4k video or high-resolution still camera been

utilized the resolution of the model would have been at the centimeter level. This resolution could have potentially proved an important utility to the structural interpretation process. Allowing the user view geometries at different angles and closely examine bed traces, the model may have served as a simulated proxy to the area itself.

Figure 10: 3D Model of the study area, merged point cloud. View is an oblique view, looking south, of the study area.

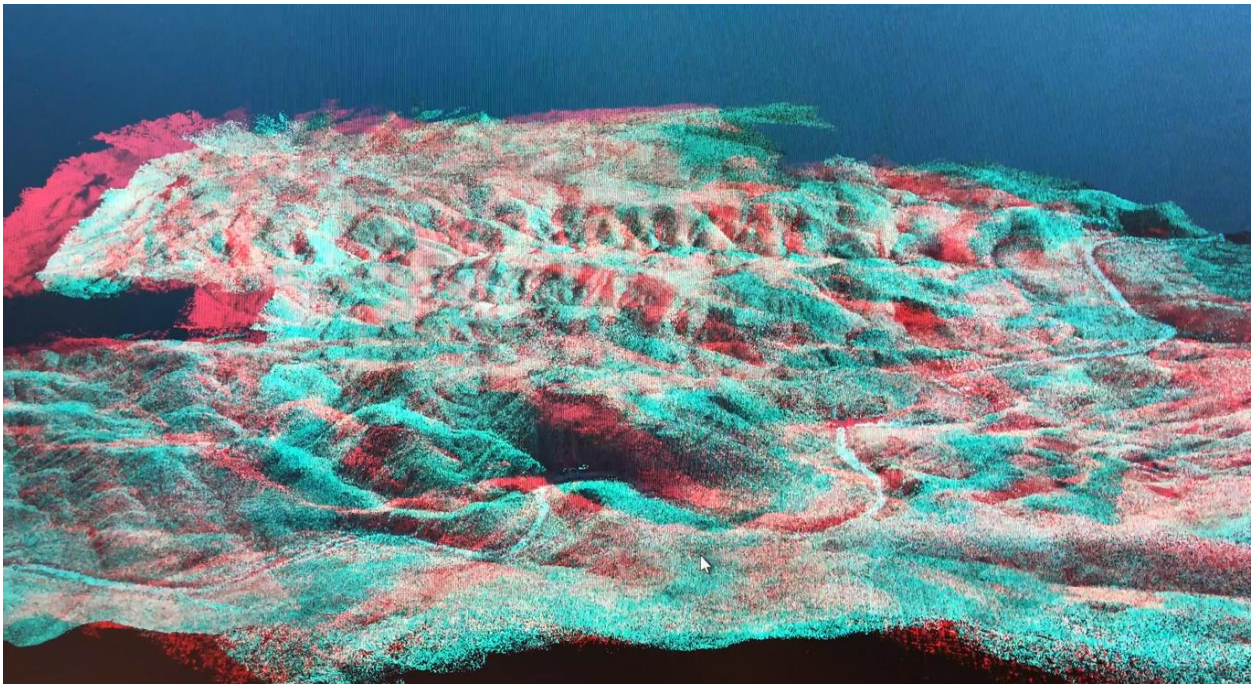

Figure 11: 3D Model of the study area displayed with red and cyan 3D visualization. View is the same as Figure 10.

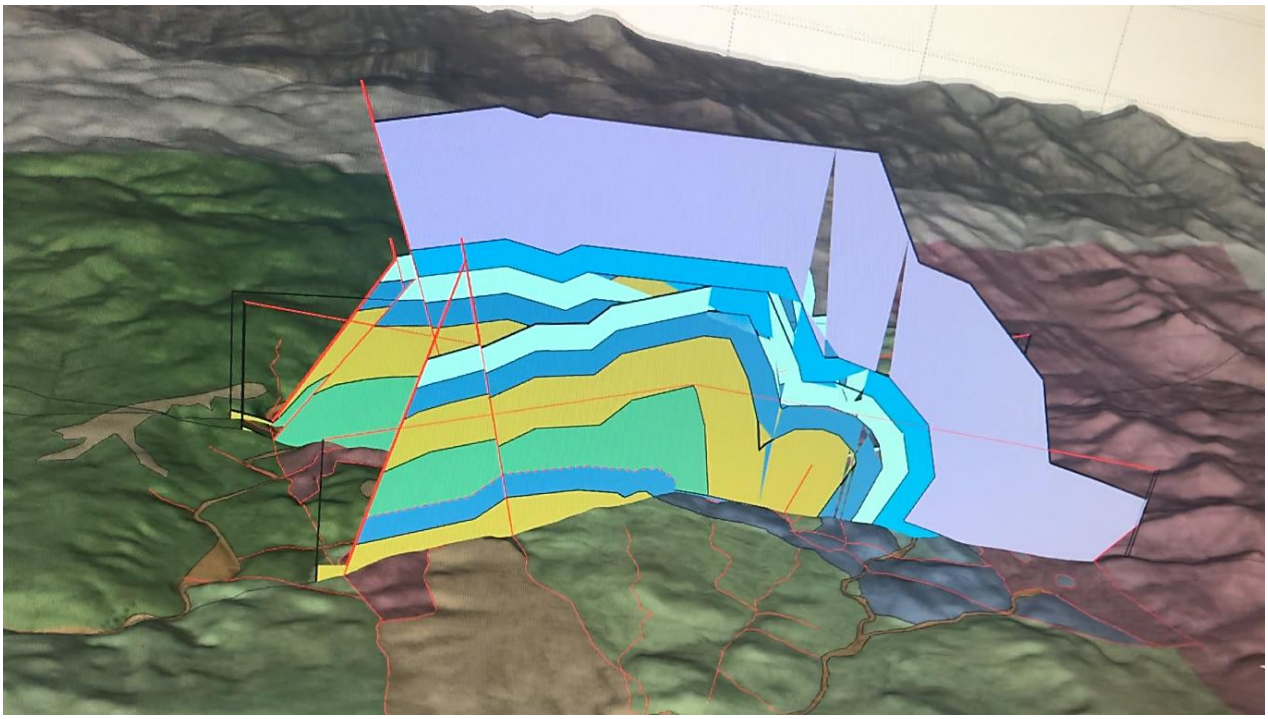

Figure 12: DEM created from 3D model overlaid with imagery and map units, with cross-section projected above and below.

5.3 Structural Geology

Page (2011) mapped the eastern part of the study area (Plate - 1) but recognized that his mapping did not fully describe the complexity of the structure. His work recognized the half klippe centered on the ranch house (Plate - 1) and folds involving the Bluff Mesa formation in the footwall of that thrust, but he did not attempt to unravel the structure to the west of the Bluff Mesa exposures. Plate – 1 illustrates my interpretation of the map scale features in the study area, and several salient points are key features of this map:

1) Tertiary gravels top several of the hills in the area and blanket a significant region in the southern part of the mapped area. These gravels lie above a conspicuous angular unconformity. To the south, in the area mapped by Ramirez (2018), a similar appearing unconformity is clearly Eocene in age because it is overlain by Eocene volcanic rocks, but the angular unconformity in the study area is almost certainly a much younger feature. That is, gravels that overlie the unconformity in the study area are poorly consolidated and contain clasts of Eocene volcanic rocks, requiring a Neogene age. Thus, these gravels are apparently erosional remnants of the Neogene basin formed in the hanging wall of the Indio fault, but subsequently exhumed by later erosion along the Rio Grande valley. For the purposes of this study, these deposits obscure parts of the Mesozoic geologic framework, confusing the local interpretation, but do, nonetheless, provide an overlap clarifying Neogene structures.

2) In the southwestern third of the mapped area a pair of oppositely dipping normal faults were recognized. These normal faults are interpreted as the northwest extensions of a pair of normal faults mapped to the south by Ramirez (2018), the Red Mountain fault to the east and the Borrego fault to the west. These normal faults are important because they disrupt an already

complex Mesozoic thrust structure, but their presence also is critical because it explains otherwise irrational juxtaposition of units.

3) The location of various exposures of lower Yucca Formation provide important indicates of the larger scale structure in the study area. Specifically, two large patches of lower Yucca in the western third of the mapped area, between the Borrego and Red Mountain normal faults, clearly lie atop upper Yucca member 2, forming two half klippen that are part of a larger thrust system that placed lower Yucca on upper Yucca member 2. Smaller klippen of this same fault are exposed just east of the Red Mountain normal fault (Figure 13), with lower Yucca laying on ridge-tops above faulted upper Yucca 2. One klippe in particular, also located east of the Red Mountain normal fault contains two windows, thus directly exposing the Upper Yucca member 2 beneath the overlying lower Yucca.

4) In the middle of the mapped area are three thrust faults, referred to from east to west as, the Mesa, Chaya, and Yucca thrust faults. The Mesa and Chaya thrust faults dip eastward at very low angles, with the Chaya thrust placing the older upper Yucca member 3 atop the younger Bluff Mesa member 1. East of the Chaya thrust fault is the Yucca thrust fault, which is a high angle thrust strictly located within the upper Yucca 3 member. These three thrust faults are important because they play an essential role in understanding the thrust system and shed light on the non-sequential repetition of units.

5) Along the southern portion of the mapped area is an east-west trending thrust fault, recognized here as the Barrow thrust fault. The Barrow thrust fault conspicuously dividing the mapped area from an intricate fold and thrust system within its hanging wall, in contrast to the homogenously dipping southern footwall. In the southwestern portion of the mapped area the Borrego and Red Mountain normal faults cut through the Barrow thrust faults. This is important

because this cross-cutting relationship clearly illustrates the overprinting of Laramide compression by Neogene extension.

6) There are two main types of fold styles in the study area, large broad folds with gentle to open geometry, and detachment folds at a variety of scales with tight to close geometry and pronounced overturning of beds on the limbs.

A) Located within the eastern half of the mapped area, east of the Yucca thrust fault and west of the Indio normal faults is an asymmetrical detachment fold. This fold was recognized by Page (2011) and consists of vertical to overturned beds east of the Yucca thrust fault (Figure 14). These overturned beds are within the upper Yucca member 3 over lain sequentially by the Bluff Mesa members 1 and 2, thus forming an overturned syncline.

B) A large broad open anticline within the upper Yucca member 2 is mapped south of the Barrow thrust fault and east of the Red Mountain normal fault. It can be inferred, that the western limb of the open anticline is covered by the previously mentioned Neogene basin fill, although the exact geologic structures remain uncertain.

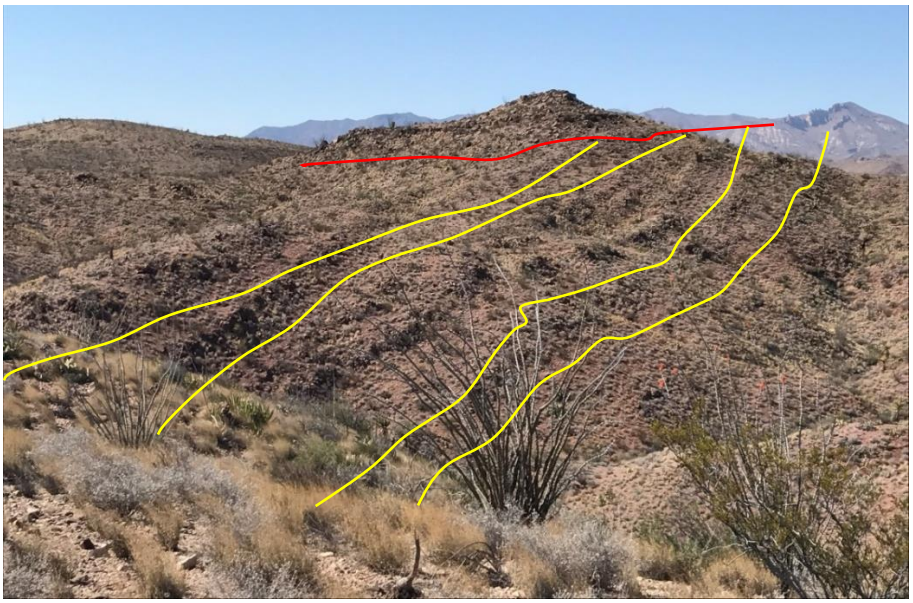

Figure 13: Truncated beds, creating an angular discordance, with the Squaw thrust (Red) placing lower Yucca on top of Upper Yucca. Yellow lines are upper Yucca trace lines. View in the central part of the mapped area looking north. Note that bedding is dipping to the left and thus, the footwall cutoff angles are opposite typical geometries that would occur beneath an east-directed thrust, indicating either out-of-sequence thrusting or a back-thrust. See text for discussion of the significance of this observation.

Figure 14: Near vertical Bluff Mesa beds as a part of the limb of a detachment fold, found west of the Indio Ranch Headquarters. Yellow lines are trace lines along strike.

5.4 Cross-sections

Two cross-sections were generated to constrain map interpretations and illustrate the 3D interpretation of the structure. The cross-sections used the DEM generate from the 3D model for the topographic profiles with the geologic map projected onto the model using the 2.5D method within *Move* software. Cross-section A-A trends across -strike (Plate - 2), along an NNE direction cutting through the northern part of the study area.

This section line was chosen specifically to cross the very low angle thrust that forms the system of lower Yucca klippen mapped across the area as well as crossing the complex fault system and folds that involve the Bluff Mesa Formation in the east. This upper thrust is the key geometric element of the major structure in the area and is interpreted as a driver for fault-related folds across the area. These structures also indicate a subsurface foreland dipping duplex with the Squaw thrust acting as the roof thrust, and it is assumed that the Barrow thrust is at a shallow depth acting as the basal thrust to the duplex. In this cross-section the Barrow thrust was placed about 50-100 meters in the subsurface. This position was inferred by projecting the Barrow thrust trace down the N dip of the fault using project to section utilities is *Move* software. Because of the interpretation of a shallow basal thrust, another cross-section we created in order to clearly depict two possible interpretation of the structures involved.

Cross-section B-B’ (Plate - 3) trends from west to east across the center of the mapped area and was chosen to cross lower Yucca klippen and the Barrow thrust. This cross-section aids in understanding the extent of the duplex as it was scaled within a shallow 50-100 meter area at depth. Because the Barrow thrust daylights in the center of the section, this cross-section was created with a 2x vertical exaggeration to depict the structures within the confined area. Note that

much of the structural complexity seen to the north is in the eroded part of this section and is therefore simplified in the section.

Cross section B-B' also resembles the an "upper plate duplex" (Pavlis, 2013), with the small foreland dipping duplex atop the upper plate of the Barrow thrust, and large open folds at depth in the footwall of the ramp flat. This occurance leads to the interpretattion of another ramp-flat geometry below the Barrow thrust, that possibly moved simutaneouly with the Barrow thrust.

Based on thmese cross-sections, two possible hypotheses were modeled. There first Model: 1 (Figure 15) restores the fold and thrust system with the removal of the slip on the Neogene normal faults. In the eastern third of the section imbricate thrusts thicken the upper Yucca member 2. In the center are the mapped Mesa thrust and the Chaya thrust, above and to the west of the basal ramp. This interpretation presents the scenario of an "upper plate duplex" (Pavlis, 2013). Because the Mesa thrust is acting as an out of sequence thrust placing younger Bluff Mesa on older Yucca. Sequentially forming a foreland dipping duplex on the upper plate.

Model: 2 (Figure 16) restores the system where the Neogene normal faults are removed and with the removal of the roof thrust or Squaw Peak thrust. In this interpretation, by removing the roof thrust, it infers that the Squaw Peak thrust overrides previously deformed rocks, thus decapitating fold and thrust structures.

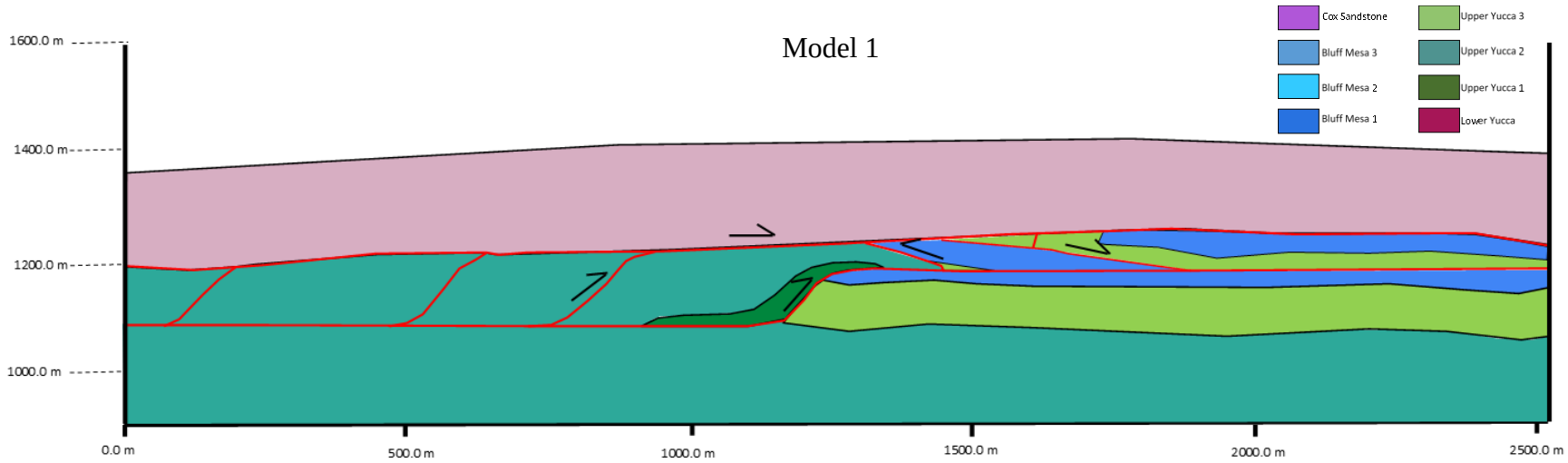

Figure 15: Model 1 is a hypothesis conveying the Squaw Peak thrust (upper thrust) and the Barrow thrust (lower thrust) moving simultaneously, thus forming an "upper plate duplex," and driven by the out of sequence Mesa thrust.

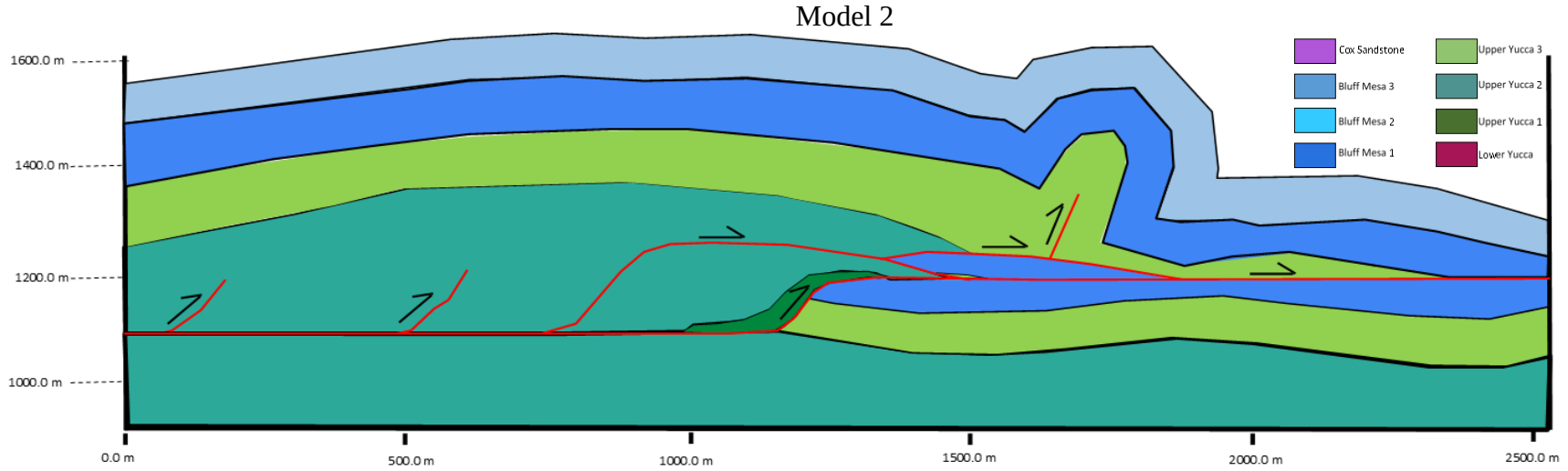

Figure 16: Model 2 is a hypothesis conveying structures forming as a result of the Barrow thrust (lower thrust) thus implying that the Squaw Peak thrust occur later decapitating folds.

5.5 Gravity Survey

Figure 17, is the Complete Bouguer anomaly which displays a smooth trend of values ranging from -0.269 to 0.331 mGals. The lower values can be interpreted the presences of less dense sandstones and shales. While the high values can be interpreted as more dense rocks such as the limestone of the Bluff Mesa formation. The map depicts relatively rapid changes in density trending within the northwest-southeast direction, alternating from low to high values. Thus, conveying the multiple faults in the area. The most significant of those being the Borrego, Red Mountain normal faults, and the Squaw Peak and Barrow thrust faults.

To further constraint the data residual gravity data found in Figure 18, focuses on more local anomalies. After over laying the mapped faults onto this map, the correlation between the two enhance certainty within fault locations, proving highly valuable for geologic interpretation. Thus, a gravity profile (Figure 19) was constructed along the cross-section A-A' (Plate - 2) in order to build a relative subsurface interpretation in correction with the known geology. An error of 0.783 was achieved after significantly establishing my structural interpretation.

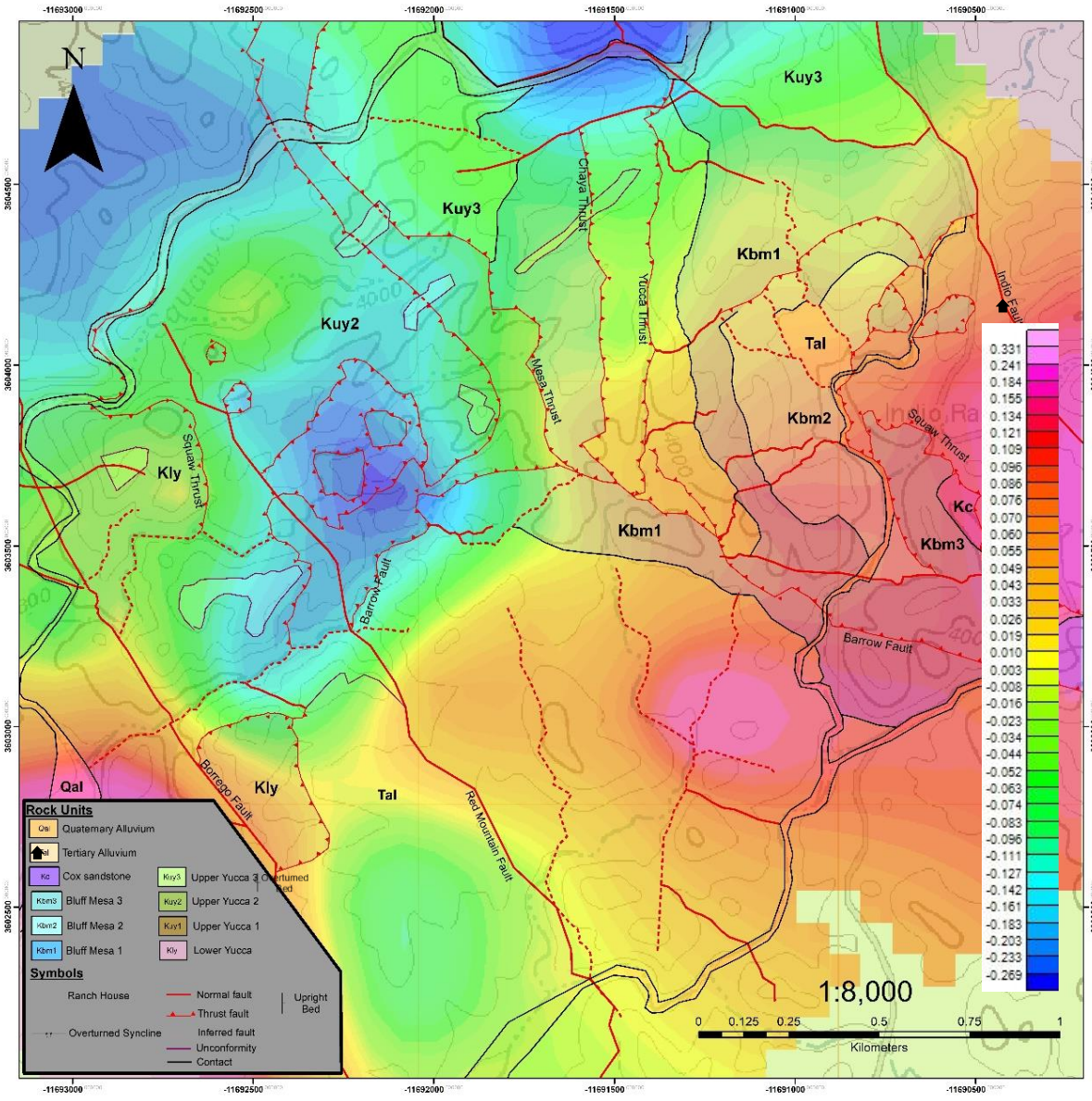

Figure 17: Geologic map overlaid by the complete bouguer anomaly over study area.

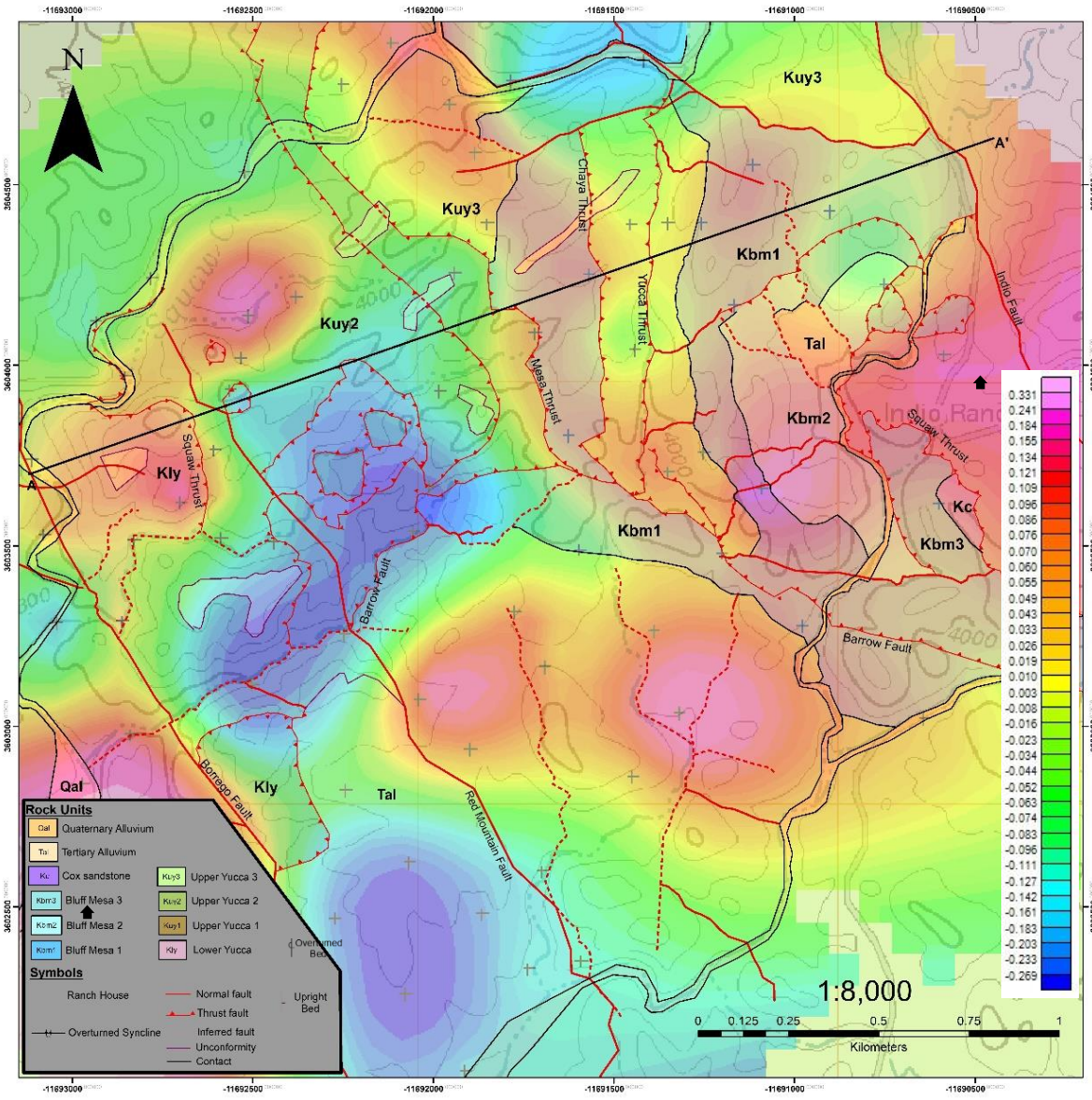

Figure 18: Map overlaid by residual gravity over study area.

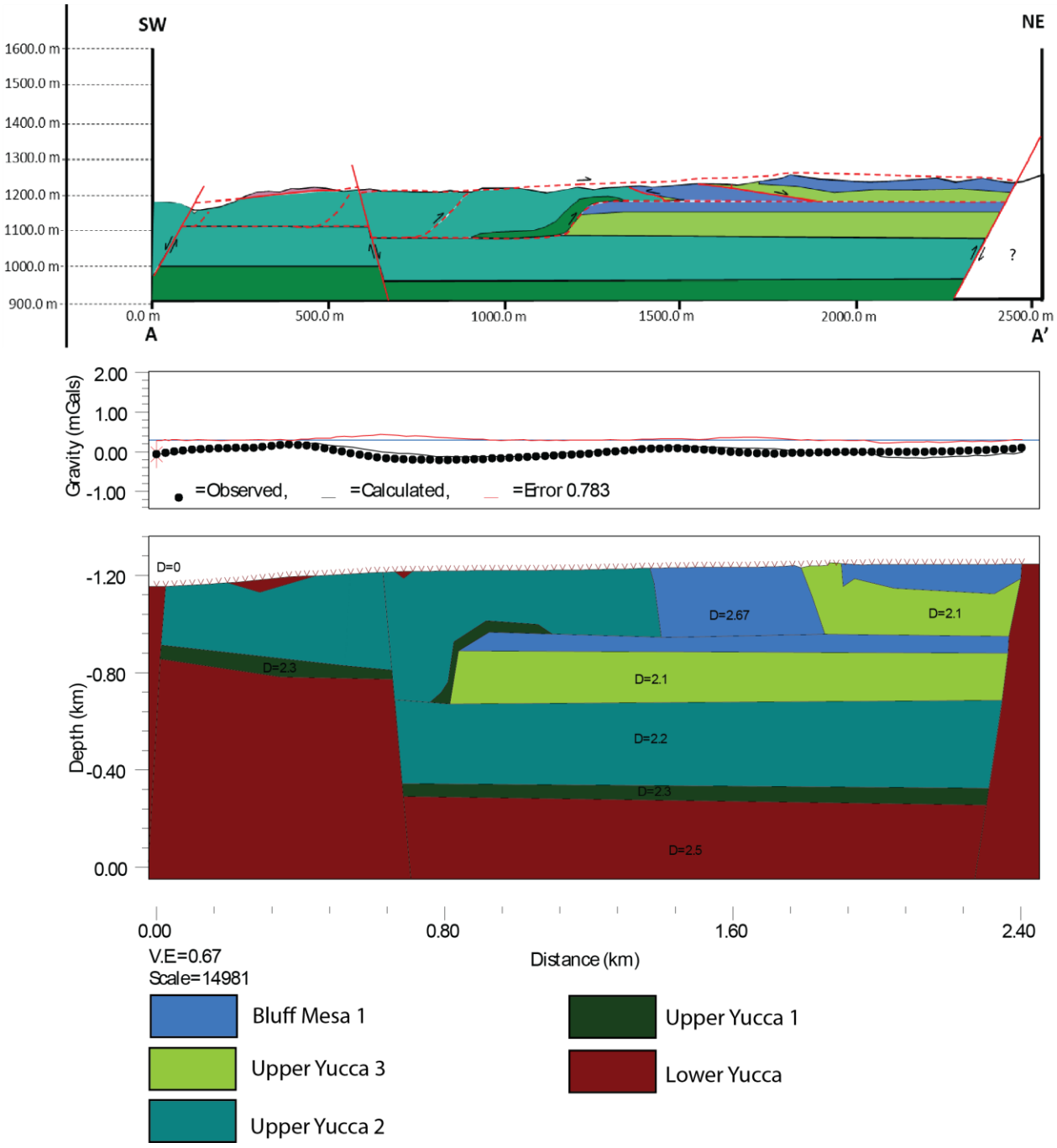

Figure 19: Gravity profile generated with an error of 0.783 between the observed and calculated gravity values. Profile was created with cross-section A-A' as a geological refence.

6. Discussion

6.1 Stratigraphy

Because the study area was too highly deformed to measure a full section of the upper Yucca formation a stratigraphic column was measured in the southern Indio Mountains, approximately 4 kilometers from the study area in collaboration with Ramirez (2018). The southern area division of the upper Yucca into three informal members proved critical for analyzing structures in the mapped area.

Comparison to the stratigraphic column measured by Page (2011) allows one assessment of the hypothesis that the Ranch House klippe and the klippen mapped in this study are remnants of the Squaw Peak thrust sheet. The measured section of the upper Yucca used by Ramirez (2018) and in this study is somewhat thinner that the 657 meter section measured by Page (2011) in the hanging wall of the Squaw Peak thrust near its type area on Squaw Peak but is much thicker than sections measured in the footwall of the Squaw Peak thrust (E.g. Page, 2011; Le, 2012). The upper Yucca section within the study area has more shale layers relative to Page's (2011) section and the measured section, which most likely contributed to the level of deformation relative to the area mapped by Ramirez (2018). Nonetheless, the general thickness of Page's (2011) section is comparable suggesting that the imbricated strata directly beneath it were derived from a similar section. Thus, all of the rocks in the mapped area are possibly allochthonous relative to rocks in the Bennet thrust sheet.

Unfortunately, this interpretation of the Squaw Peak thrust within the mapped area poses a possible contradiction, where thrust sheet distinction becomes complicated. If the thrust associated with the klippen is in fact the Squaw Peak thrust, then that would infer the underlying rock units are within the footwall of the Squaw Peak thrust, yet Ramirez (2018) interpreted the

stratigraphic column to be within the hanging wall of the Squaw Peak thrust. Thus, this contradiction implies two possibilities: 1) The correlation to the Squaw Peak thrust is incorrect, and this fault is a part of a higher level thrust sheet. 2) The correlation to the Squaw Peak thrust is correct, yet the hanging wall is juxtaposed on to similar basinal deposits.

6.2 Structures

From the beginning of this project it was apparent that the area was highly deformed. Initially the north western part of the area raised questions, especially from a map view perspective. The area displays rapid dip changes, bed truncations, and repeated sections at small scales of 10's 100's of meters. After completion of the mapping, however a structurally very low angle Chaya thrust adjacent to a the out of sequence Mesa thrust at the center of the map presented issues when building the cross-sections and interpretation. The Mesa thrust is particularly problematic. This thrust trends northeast-southwest and is interpreted here to be an out-of-sequence thrust fault, placing the younger Bluff Mesa member 1 atop the older upper Yucca member 2. This younger on older occurrence is typical of out of sequence thrusting, but also occurs in normal faulting. The Chaya and the Mesa thrusts are viewed to be the kinematic drivers of this small fold and thrust system.

This system is truncated by the overlying Squaw Peak thrust. Underwood (1962) initially interpreted the Squaw Peak thrust as a back thrust, but Page (2011) showed that the slip direction, footwall and hanging wall cutoffs, and trend of the thrust were inconsistent with that interpretation. Nonetheless, Page (2011) interpreted the western Squaw Peak thrust, the Ranch House klippe, to be a basal thrust, despite his interpretation that the structure is the roof thrust for an underlining thrust duplex.

The results of this study suggest a more complex structure than envisioned by Page (2011). Assuming the low-angle fault that forms the base of the klippen dispersed throughout the mapped area is the Squaw Peak thrust, the structures beneath the thrust are very different than the large-scale duplex that Page (2011) inferred to the east of the Indio fault. The interpretation of a continuous, low-angle Squaw Peak thrust exhumed across the mapped area is supported by the klippen found across the study area, including the Ranch House klippe. All of these klippen carry lower Yucca in the hanging wall, like the Squaw Peak thrust. What is distinct in the study area, however, is that less than 200 meter below the Squaw Peak thrust is a basal floor thrust of the duplex, the Barrow thrust fault. This inference results in a thin, complexly imbricated zone between the two thrust with a shallow fold and thrust system, which is significantly different from the Mesozoic structure within the Indio fault footwall.

Large duplexes are associated with contractional systems, where a thrust fault ramps upward from a basal thrust, and as contraction continues and stress propagate forward imbricate faults form and join at a roof thrust above. In the Indio foot wall, a large duplex is inferred by Page (2011). Yet in the case of the Indio hanging wall, a small duplex is interpreted here. Small, thin duplexes are associated with out of sequence thrust faulting, and parallel ramp flats faults moving simultaneously (Pavlis, 2013) forming a small duplex on the upper plate (Figure 20). An example is the Moine Thrust system in Scotland where it has been interpreted to have a small duplex within a larger foreland dipping thrust system. This system contains a small duplex within a larger thrust system therefore complicating the system (Johnstone, 1989) (Figure 21). This type of structures can be easily interpreted as foreland dipping duplex (Pavlis, 2013), when in fact their kinematic origin is different.

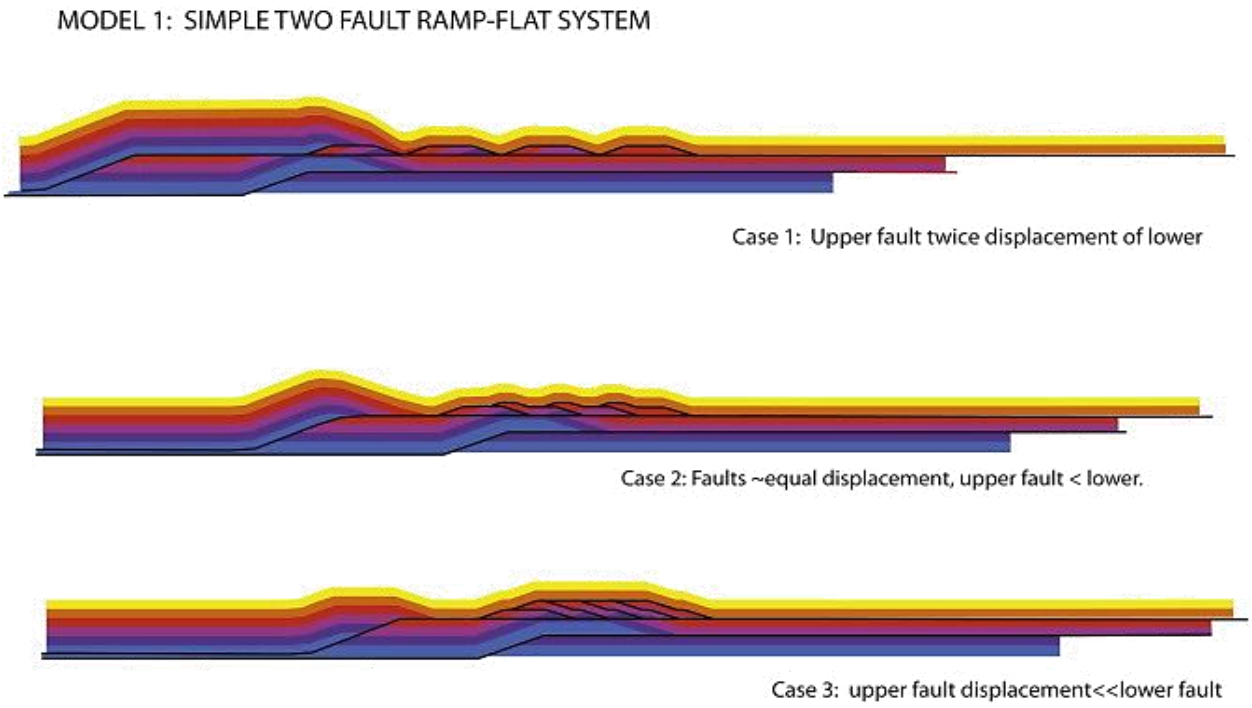

Figure 20: Model from Pavlis (2013) with varying cases in which this study favors case 3.

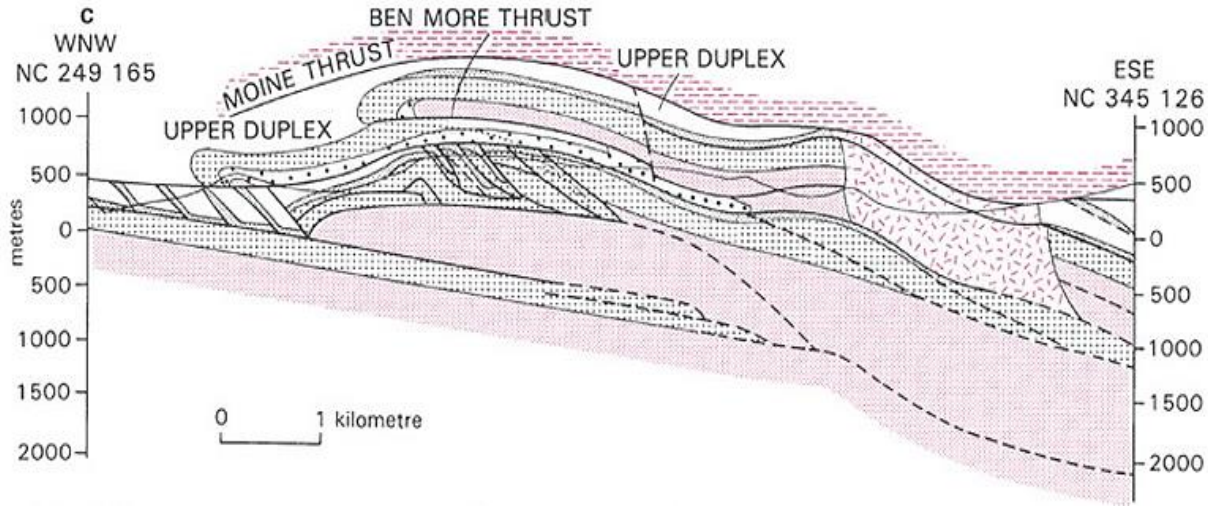

Figure 21: Cross-section of the Moine thrust system in Scotland. Modified from Johnstone (1989).

Pavlis (2013) generated kinematic models suggesting various "upper plate duplex" geometries resulting from out of sequence faulting. For each model various cases were developed in relation to variations in displacement speed between the upper and lower faults. In the circumstance of the Indio hanging wall, the study area is similar to Pavlis' (2013) *Model 1: Case 3*. The interpretation of an "upper plate duplex," within this study area, is further complicated by the stratigraphy and supports the hypothesis that this area is in fact a higher thrust and possibly does not correlate to the Squaw Peak thrust.

6.3 3D Model

The 3D model was intended to aid the mapping process, as the area was structurally complex and should have benefited from the ability to visually orient the landscapes and visualize, in 3D, both beds and structural orientations. The concept of 3D modeling is an advancement in the geologic community, especially a model as large as the one built for this project; by which ultimately the goal of the 3D model was to map the line data on the model for interpretation. Unfortunately, due to the relatively low resolution of the model brought on by my use of relatively low-resolution imagery (standard HDTV video), the model was too low resolution to provide insight beyond what could be gained from 0.5 meter resolution orthoimagery. Many factors may have played a part in the reduced resolution, from the height and speed of the drone, time of day, or the conversion from video to jpeg. Nonetheless, it is clear that the great problem was choice of the low-resolution video format. Had we used a standard camera or higher resolution video, it is likely the results would have been far better.

The large scale of the area relative to 3D modeling also proved to be time consuming, as the *PhotoScan* software took between days to weeks to fully process as most models consisted

on average 700-850 photos. In addition to the final step of combining all the points clouds, within the *CloudCompare* software, requiring significant processing time.

The process in creating the model was very long and could have been another project in itself. Dividing the area into smaller models and eventually combining them all heavily relied on the point markers. For future projects it is recommended that point markers are made exceedingly visible, and uniquely distinguishable. When combining the point clouds these markers not only providing a geographical reference but a great visual point to precisely pick points on multiple images to match up and merge the various point clouds. These markers also proved to be a great spatial reference when navigating the 3D model.

6.4 Gravity Survey

Although the gravity survey, produce a small anomaly variation for this area, the results proved to be visually informative and was very helpful when refining the final map. In particular, the dense Bluff Mesa and lower Yucca stood out and brought more understanding to fault locations. The rapid transitions between gravity lows and highs correlate well with the mapped faults. In addition, the modeled gravity profile along cross-section A-A' provided support for the subsurface interpretation. This study is the first gravity survey that has been done in the Indio Mountains, where hilly terrain and lack of roads proved quite difficult for data collection. On the other hand, because a gravity base was established at the Indio Ranch Headquarters, continued gravity surveys are recommended as this area, because density contrasts between units are clearly sufficient to produce recognizable anomalies that could be used to constrain structure.

7. Conclusion

An updated geologic map of the western Indio Mountains shows a complex, previously unmapped fold and thrust system. This thrust system is capped by a low-angle thrust placing lower Yucca Formation on complexly imbricates upper Yucca strata and floored by a thrust sheet with gently homoclinal dipping upper Yucca in its footwall. The upper thrust in tentatively correlated to the Squaw Peak thrust. Identification of the exact thrust sheet, however, is complicated by faulting resulting in the inability to generate a stratigraphic column within the area itself. This creates ambiguity in truly correlating to previous works in the area.

Field mapping, gravity survey, and 3D modeling collectively constrained the geologic interpretation of the area to most likely be an example of an "upper plate duplex." In this hypothesis the out of sequence Mesa fault is interpreted to be a critical feature. Research by Ramirez (2018) to the south aided this study with recognition of two Neogene structures, the Borrego and Red Mountain, normal faults continuing northward into the mapped area. An updated map of the area between these two studies may shed light on regional geologic correlations and fill in the gaps of the Indio normal fault's hanging wall. A larger sturdy area map within the Indio hanging wall may aid in understanding regional tectonics and structural complexities. Also, to entirely confirm these structures a seismic survey would be optimal so subsurface interpretation, yet due the areas difficult accessibility and terrain would a long and grueling task. However, future studies may be complicated by stratigraphy, unless a reliable stratigraphic column relative to the area is generated to adequately identify thrust sheets within the Indio hanging wall.

8. References

Anderson, T. H., & Schmidt, V. A., 1983, The evolution of Middle America and the Gulf of Mexico–Caribbean Sea region during Mesozoic time: Geological Society of America Bulletin, v. 94, p. 941-966.

Anderson, T. H., & Silver, L. T., 2005, The Mojave-Sonora megashear—Field and analytical studies leading to the conception and evolution of the hypothesis: Geological Society of America Special Papers, v. 393, p. 1-50.

Beauchamp, W., Barazangi, M., Demnati, A., and El Alji, M., 1997, Inversion of synfrift normal faults in the High Atlas Mountains, Morocco: The Leading Edge, p. 1171-1175.

Brush, J. A., 2015, Evaluating methods of field-based 3D visualization and their application to mapping metamorphic terranes: An example from the Panamint Mountains, California, [Master's thesis]: The University of Texas at El Paso. 143 p.

Campbell, D. H., 1980, The Yucca Formation-Early Cretaceous continental and transitional environments, southern Quitman Mountains, Hudspeth County, Texas. In Trans-Pecos region: New Mexico Geol. Soc. Guidebook, 31st Field Conf, p. 159-168.

Carciumaru, D., & Ortega, R., 2008, Geologic structure of the northern margin of the Chihuahua trough: Evidence for controlled deformation during Laramide Orogeny: Boletín de la Sociedad Geológica Mexicana, v. 60, p. 43-69.

Caumon, G., Collon-Drouaillet, P., De Veslud, C. L. C., Viseur, S., & Sausse, J., 2009, Surface-based 3D modeling of geological structures: Mathematical Geosciences, v. 41(8), p. 927-945.

Chandra, S., Gideon, N. D., Chaturvedi, C., & Rana, M. S., 2006, Basin Inversion and

Hydrocarbon Entrapment in Ramnad & Palk Bay Offshore of Cauvery Basin, India: In 6th International Conference & Exposition on Petroleum Geophysics, Kolkata.

Chapple, W. M., 1978, Mechanics of thin-skinned fold-and-thrust belts: Geological Society of America Bulletin, v. 89(8), p. 1189-1198.

Dahlen, F. A., 1984, Noncohesive critical Coulomb wedges: An exact solution, Journal of Geophysical Research: Solid Earth, v. 89(B12), p. 10125-10133.

Dickinson, W. R., & Lawton, T. F., 2001, Carboniferous to Cretaceous assembly and fragmentation of Mexico: Geological Society of America Bulletin, v. 113, p. 1142-1160.

Fitz-Díaz, E., Lawton, T. F., Juárez-Arriaga, E., & Chávez-Cabello, G., 2017, The Cretaceous-Paleogene Mexican orogen: Structure, basin development, magmatism and tectonics: Earth-Science Reviews.

Fox, F. G., 1969, Some principles governing interpretation of structure in the Rocky Mountain orogenic belt: Geological Society, London, Special Publications, v. 3, p. 23-41.

Fox, M., 2016, Depositional and Structural controls on Fluvio-Deltaic and Lacustrine strata of the Upper Yucca Formation in the Indio Mountains, West Texas, [Master's Thesis]: University of Texas at El Paso.

Giambiagi, L., Bechis, F., García, V., & Clark, A. H., 2008, Temporal and spatial relationships of thick-and thin-skinned deformation: A case study from the Malargüe fold-and-thrust belt, southern Central Andes.Tectonophysics, v. 459, p. 123-139.

Haenggi, W. T., 2001, Tectonic history of the Chihuahua trough, Mexico and adjacent USA, Part I: the pre-Mesozoic setting: Boletin de la Sociedad Geologica Mexicana, v. 54, p. 28-66.

Haenggi, W. T., 2002, Tectonic history of the Chihuahua trough, Mexico and adjacent USA,

Part II: Mesozoic and Cenozoic: Boletin de la Sociedad Geologica Mexicana, v. 55, 38-94.

Johnstone, G. S., & Mykura, W., 1989, British regional geology: the Northern Highlands of Scotland, HM Stationery Office, v. 2, p. 219.

Li, X., 2015, Sedimentological, Stratigraphic, and Diagenetic Analysis of Microbialite-Bearing Lacustrine Rift Sequence within the Lower Cretaceous Yucca Formatiom, Indio Mountains, West Texas, [Master's thesis]: The University of Texas at El Paso, 136 p.

McClay, K. R., & Buchanan, P. G., 1992, Thrust faults in inverted extensional basins. In Thrust tectonics, Springer, Dordrecht. p. 93-104.

Morley, C. K., 1988, Out-of-sequence thrusts: Tectonics, v. 7, p. 539-561.

Page, S. J., 2011, Fold-thrust system overprinting syn-rift structures on the margin of an inverted rift basin: Indio mountains, west Texas, [Master's thesis]: The University of Texas at El Paso, 68 p.

Pavlis, T. L., 2013, Kinematic model for out-of-sequence thrusting: Motion of two ramp-flat faults and the production of upper plate duplex systems: Journal of Structural Geology, v. 51, p. 132-143.

Pavlis, T. L., Brush, J. A., Hurtado Jr, J. M., & Knott, J. R., 2015, Evaluating methods of field-based 3D visualization and their application to mapping metamorphic terranes: An example from the Panamint Mountains, California.

Pavlis, T. L., Chapman, J. B., Bruhn, R. L., Ridgway, K., Worthington, L. L., Gulick, S. P., & Spotila, J., 2012, Structure of the actively deforming fold-thrust belt of the St. Elias orogen with implications for glacial exhumation and three-dimensional tectonic processes: Geosphere, v. 8(5), p. 991-1019.

Poole, F. G., Perry, W. J., Madrid, R. J., & Amaya-Martínez, R., 2005, Tectonic synthesis of the Ouachita-Marathon-Sonora orogenic margin of southern Laurentia: Stratigraphic and structural implications for timing of deformational events and plate-tectonic model: Geological Society of America Special Papers, v. 393, p. 543-596.

Russell, H. A. J., Thorleifson, L. H., & Berg, R. C., 2013, Overview-3D geological mapping: developing more widespread adoption by geological survey organizations: Three-Dimensional Geological Mapping, v. 7.

Sedek, M. S., & Al Mahdy, O. M. M., 2013, Inverted basin analysis and geological modeling, Razzak oil field, Western Desert, Egypt: Arabian Journal of Geosciences, v. 6, p. 2261-2283.

Smith, J. F., 1940, Stratigraphy and structure of the Devil Ridge area, Texas: Geological Society of America Bulletin, v. 51, p. 597-637.

Stojakovic, V., 2008, Terrestrial photogrammetry and application to modeling architectural object: Architecture and Civil Engineering, v. 6, n. 1, p. 113-125.

Tibaldi, A., & Bonali, F. L., 2018, Contemporary recent extension and compression in the central Andes: Journal of Structural Geology, v. 107, p. 73-92.

Underwood Jr, J. R., 1980, Geology of the Eagle Mountains, Hudspeth County, Texas. *in* Trans-Pecos region: New Mexico Geological Society, 31st Field Conference Guidebook, p. 183 to 193.

Yang, F. L., Xu, X., Zhao, W. F., & Sun, Z., 2011, Petroleum accumulations and inversion structures in the Xihu depression, East China Sea Basin: Journal of Petroleum Geology, v. 34(4), p. 429-440.

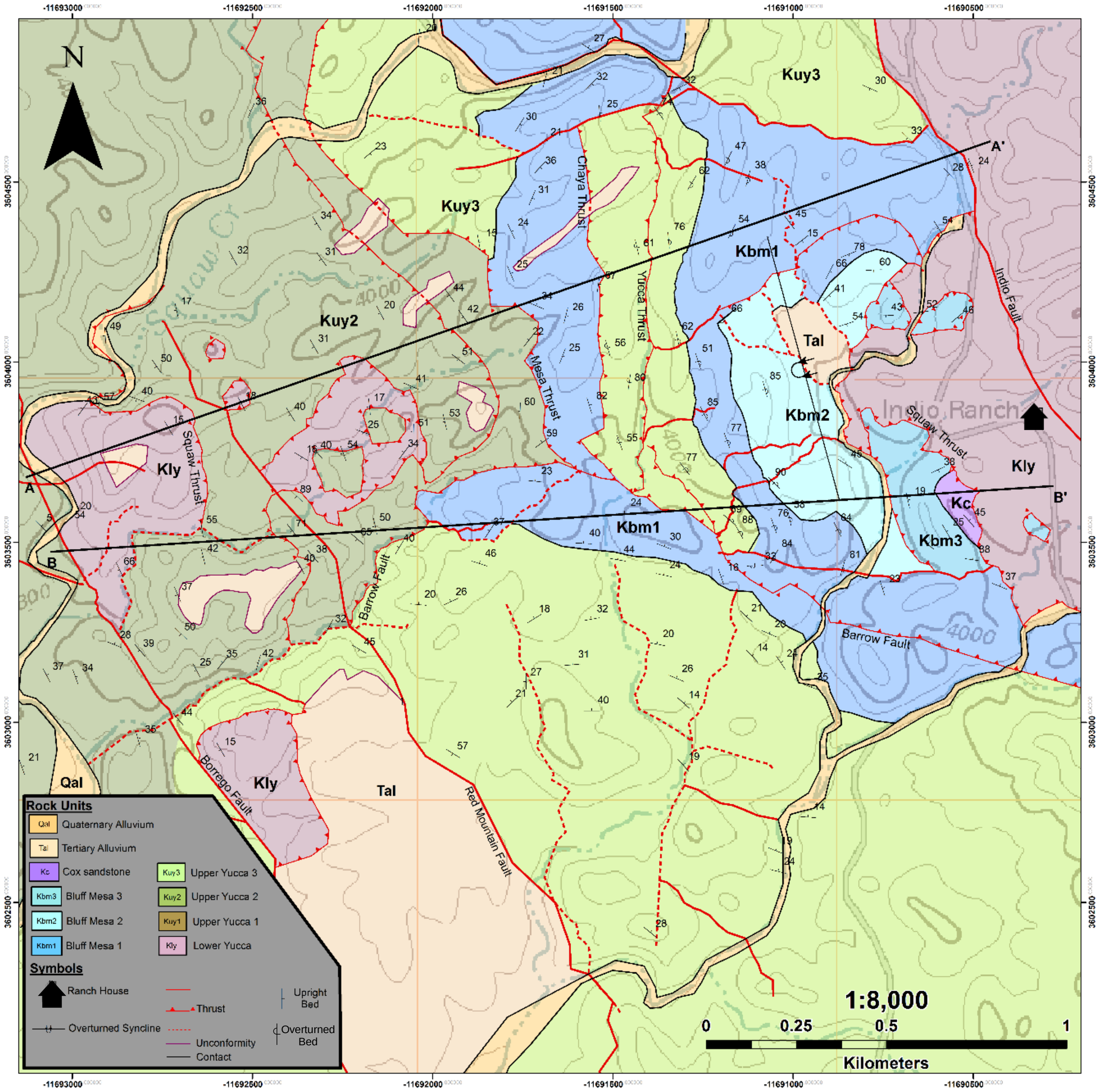

Plate - 1: Geologic map of the hanging wall, west of the Indio normal fault.

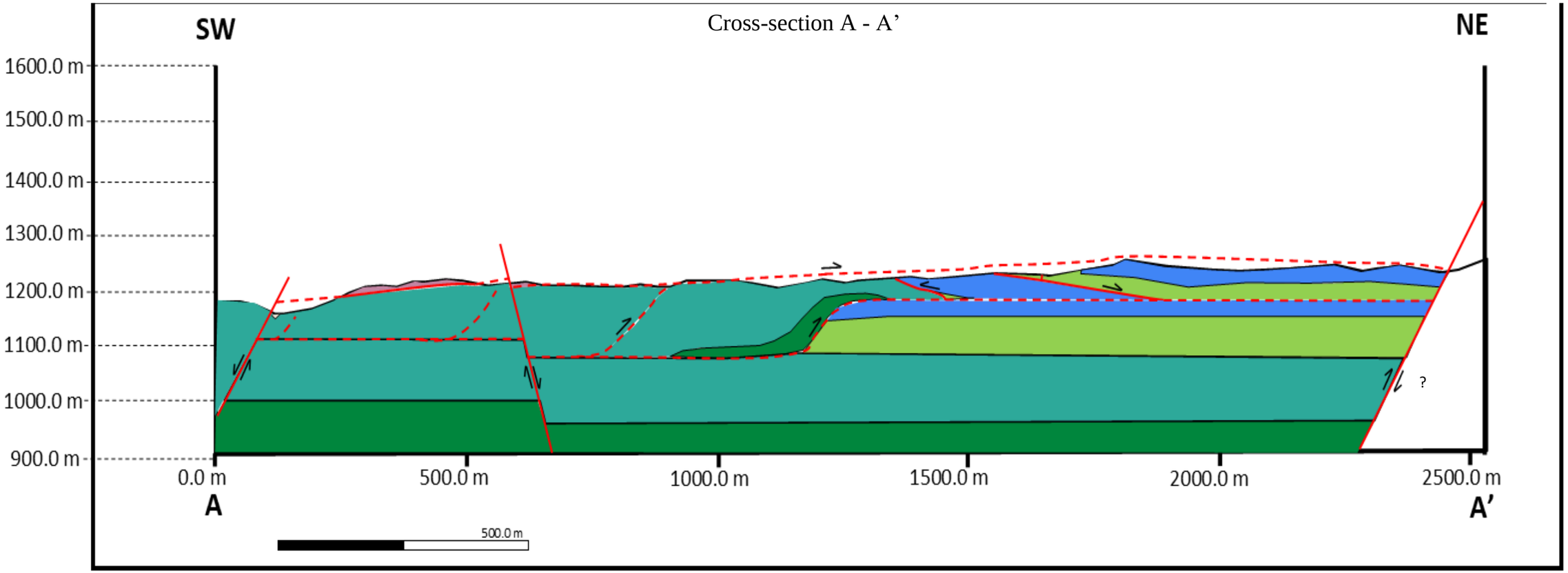

Plate - 2: (A) Cross-section A-A’ displaying the Squaw Peak thrust projecting in the air the Yucca Formation over the underlying duplex.

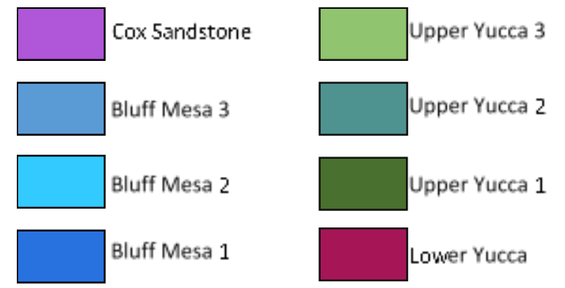

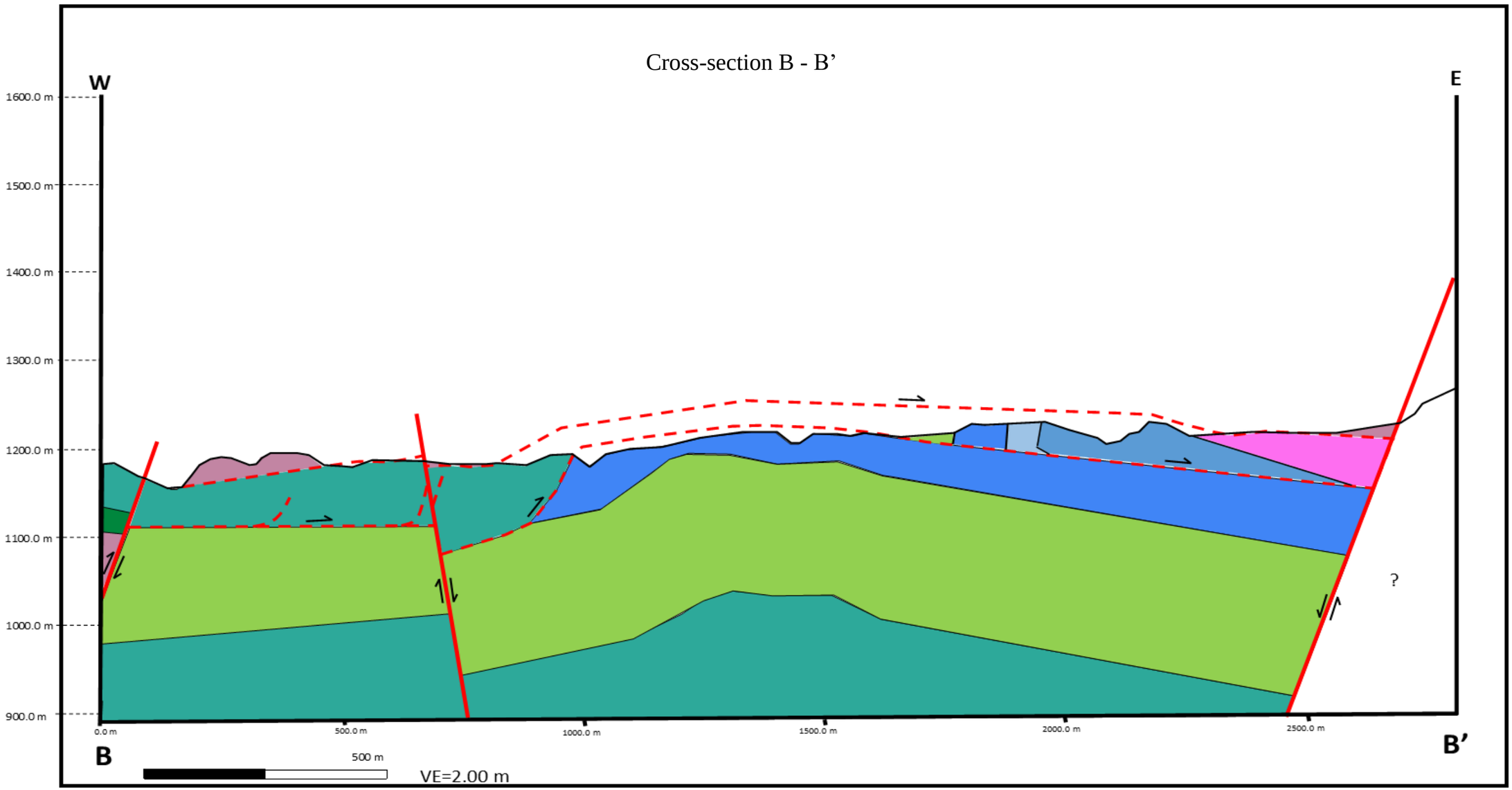

Plat – 3: Cross-section B-B’ with vertical exaggeration in order to illustrate the minimal amount of space between the Squaw Peak thrust and the Barrow thrust.

Vita

Myra Guerrero, a born and raised El Paso native, obtained her Bachelors of Science in Geology from the University of Texas at El Paso in May of 2015 making her the first in her family to attend and graduate from a university. Immediately after being awarded her degree, she applied to UTEP's graduate program in Geological Sciences where she focused on structural geology. As a student, she also worked as a GIS Specialist and aspires to remain in that field.

Myra earned her Masters of Science in Geological Sciences in May 2017.

Contact Information: Guerrero.myra@gmail.com

This thesis/dissertation was typed by Myra Guerrero.